A developmental brain-wide screen identifies retrosplenial cortex as a key player in the emergence of persistent memory

Abbreviated Title: Circuit mechanisms underlying infantile amnesia

Authors: Benita Jin[1,2], Michael W. Gongwer[1,3,4], Lilit Ohanian[1], Lucinda Holden-Wingate[1], Bryan Le[1], Alfonso Darmawan[1], Yuka Nakayama[1], Sophia A. Rueda Mora[1] and Laura A. DeNardo[1,5]*

1. Department of Physiology, University of California Los Angeles, Los Angeles, CA 90095

2. Molecular Cellular and Integrative Physiology Interdepartmental Program, University of California Los Angeles, Los Angeles, CA 90095

3. Neuroscience Interdepartmental Program, University of California Los Angeles, Los Angeles, CA 90095

4. Medical Scientist Training Program, University of California Los Angeles, Los Angeles, CA 90095

5. Department of Neurobiology, University of California Los Angeles, Los Angeles, CA 90095

*Address correspondence to: ldenardo@ucla.edu

Number of pages: 33

Numbers of figures: 6 main, 6 supplemental

Number of tables: 2

Keywords: infantile amnesia, memory, retrosplenial cortex, neural circuits, brain clearing, light sheet fluorescence microscopy

Summary: 150 words

Introduction: 571 words

Discussion: 1642 words

Summary

Memories formed early in life are short-lived while those formed later persist. Recent work revealed that infant memories are stored in a latent state. But why they fail to be retrieved is poorly understood. Here we investigated brain-wide circuit mechanisms underlying infantile amnesia in mice. We performed a screen that combined activity-dependent neuronal tagging at different postnatal ages, tissue clearing and light sheet microscopy. We observed striking developmental transitions in the organization of fear memory networks and changes in the activity and functional connectivity of the retrosplenial cortex (RSP) that aligned with the emergence of persistent memory. 7 days after learning, chemogenetic reactivation of tagged RSP ensembles enhanced memory in adults but not in infants. But after 33 days, reactivating infant-tagged RSP ensembles recovered forgotten memories. These studies show that RSP ensembles store latent infant memories, reveal the time course of RSP functional maturation, and suggest that immature RSP functional networks contribute to infantile amnesia.

Introduction

Infantile amnesia describes a process wherein episodic memories formed early in life are rapidly forgotten[1–3]. In contrast, memories formed later can last for decades. In humans, memories become persistent around age five[4]. Infantile amnesia is not a uniquely human phenomenon[5,6]. In rodents, memories become persistent during the fourth postnatal week[7–11]. But even though early formed memories cannot be consciously recalled, they can influence later experiences by promoting the maturation of learning systems and altering the mechanisms of later memory encoding[12–14]. Their continuing influence suggests that early-formed memories leave an enduring trace in the brain.

Several studies showed that infant memories are not erased but rather inaccessible. Forgotten memories leave a molecular trace in the amygdala[15]. Providing strong reminders of the original memory[13,16,17] or optogenetically reactivating infant memory ensembles in the hippocampus[11] can recover lost infant memories. Importantly, early adversity such as neglect or abuse can accelerate the development of emotional memory systems, ending the period of infantile amnesia prematurely[18,19]. Early adversity is a major risk factor for developing mental health disorders, suggesting that infantile amnesia may actually protect against the emergence of problematic behaviors[7,20]. Despite their importance for brain and behavioral development, how infant memories are stored and why they remain inaccessible remains poorly understood.

In adults, initial memory encoding in the hippocampus is followed by a period of consolidation during which episodic memories come to be stored in distributed networks across the brain[21]. Memory consolidation and retrieval involves coordinated activity of numerous regions including the prefrontal cortex, temporal cortical association areas, medial and anterior thalamic nuclei, and retrosplenial cortex (RSP)[21–23]. Long range connectivity amongst these regions continually refines throughout postnatal development until early adulthood[24–26]. It is therefore possible that developmental remodeling of the long-term memory networks render infant memories inaccessible. But little is known about the organization of memory networks in the developing brain and how they change with age. To date, mechanistic studies of infantile amnesia have focused on the hippocampus, showing that infantile amnesia is associated with naturally elevated hippocampal neurogenesis[9] and immature hippocampal synapses[13]. As such, we have only limited understanding of which aspects of brain circuit development are associated with the emergence of persistent memories.

Here we set out to investigate why infant memories become inaccessible. We considered two potential models. In the first, the infant brain may use different circuits to store and retrieve memories that are no longer used in adulthood. In the second, the same circuits are involved but memories are stored in a different way. We designed a developmental screen to distinguish between these possibilities. By performing contextual fear conditioning, whole-brain activity-dependent neuronal tagging[27–29] at different postnatal ages, tissue clearing, light sheet fluorescence microscopy, and high throughput computational analyses[30], we identified key brain regions whose activity and functional connectivity change significantly during memory retrieval across development. Our analyses indicated that while similar regions are involved in memory retrieval over development, functional connectivity amongst those regions changes significantly between infancy and adulthood. RSP emerged as a key region whose functional maturation closely aligns with changes in memory persistence. Then, in targeted functional studies, we discovered that 1) that memory ensembles in RSP are more stable in adults compared to juveniles and infants, 2) that chronically reactivating RSP memory for a week after learning ensembles enhances memory in adults but not in infants, and 3) that after 33 days, reactivation of infant-tagged RSP ensembles can recover infant memories.

Results

66 **A brain-wide screen to identify neural signatures of infantile amnesia**

67 Using an established protocol for modeling infantile amnesia[8,9,11], we performed contextual fear
68 conditioning (CFC) in mice when they were infants (postnatal day (P) 17), juveniles (P25), or
69 adults (P60). In separate cohorts of mice, we tested the strength of their fear memory 1 day (d)
70 or 7d after CFC by placing mice in the original training context and measuring freezing behavior
71 (Figure 1A). While mice of all ages exhibited robust freezing during CFC and the 1d memory
72 retrieval test, mice trained as infants froze significantly less than adults and juveniles during a
73 7d memory retrieval test (Figure 1B).
74
75 In our developmental screen, we combined activity-dependent tagging, tissue clearing and light
76 sheet fluorescence microscopy to screen for developmental changes in brain-wide cellular
77 activation patterns during memory retrieval (Figure 1C). We labeled activated neuronal
78 populations using Targeted Recombination in Active Populations (TRAP2: *Fos*$^{icre\text{-}2A\text{-}ERT2}$)[28,29], in
79 which the Fos promoter drives expression of tamoxifen-inducible Cre recombinase. We crossed
80 TRAP2 to the Ai14 Cre reporter line[31] so all TRAPed neurons could be labeled with a red
81 fluorophore. We performed CFC in infant, juvenile or adult *TRAP2;Ai14* mice. One day later, we
82 TRAPed fear memory-activated neurons by pairing re-exposure to the training context with a
83 tamoxifen injection. We chose to TRAP 1d instead of 7d memory retrieval because infant mice
84 still freeze 1d after CFC. This allowed us to relate neuronal activation patterns to freezing
85 behavior while comparing the neural signatures underlying retrieval of infant memories that
86 would fade vs. juvenile and adult memories that would persist. A week after TRAPing we
87 perfused mice, immunostained for tdTomato and rendered brains transparent using the Adipo-
88 Clear protocol[32]. We then imaged TRAPed cells in intact brain hemispheres using light sheet
89 fluorescence microscopy, automatically quantified the number of TRAPed cells per brain region,
90 and compared the resulting patterns of neuronal activation across age groups (Figure 1C).
91
92 First, we investigated whether brain regions were differentially activated during memory retrieval
93 over development (P17–P60). To do this, we calculated the number of TRAPed cells per brain
94 region as a fraction of the total TRAPed cells counted per brain. Cortical association areas,
95 regions in the hippocampal formation (HPF), and dorsal polymodal thalamic nuclei (DORpm)
96 had high fractional counts in adults compared to infants and juveniles whereas nuclei in the
97 hypothalamus and midbrain had higher fractional counts in infants compared to juveniles and
98 adults (Figure 1D,E). Cortical association areas, including the anterior cingulate area (ACA) and
99 RSP, HPF, and DORpm play key roles in memory consolidation[21,33–37]. These findings suggest

100 that maturation of regions involved in long-term memory in adults contributes to developmental
101 transitions in memory persistence.
102
103 **Developmental changes in short-term fear memory network organization**
104 To better understand which brain regions contribute to the behavioral expression of fear
105 memories across development, we conducted a partial least-squares (PLS) analysis[38] of
106 TRAPed cells across brain regions. These analyses identify latent variables that maximally
107 differentiate high versus low freezing levels during 1d memory retrieval. Bootstrap ratios (or
108 saliences) from the PLS analysis were used to determine the extent that individual regional
109 activation (based on numbers of TRAPed cells) contributed to the ability to distinguish freezing
110 levels among mice within each age group. We identified regions contributing to significant
111 contrasts by thresholding salience values at 3, which corresponds to P=0.01 (Figure 1F–H). In
112 all age groups, distinctions between freezing levels were primarily driven by TRAPed ensembles
113 in ACA, RSP, lateral septum (LSX), entorhinal cortex (ENT), and the lateral zone of the
114 hypothalamus (LH). This suggests that over development, similar regions are involved in the
115 behavioral expression of conditioned fear during 1d fear memory retrieval.
116
117 Memory retrieval and consolidation involves coordinated activity across brain regions.
118 Interregional functional connectivity strength is often estimated by assessing co-variance in
119 activity across brain regions[38,39]. In many brain regions, long-range connectivity continually
120 refines until early adulthood[24–26]. We therefore hypothesized that these structural changes would
121 produce distinct patterns of functional connectivity underlying 1d fear memory retrieval in
122 different stages of development. To examine this, we computed interregional correlations based
123 on the number of TRAPed cells and compared across the age groups. Based on our findings
124 that cortical association areas and DORpm are more highly activated during memory retrieval in
125 adults, we focused our covariance analysis on these and connected regions.
126
127 This analysis revealed an overall decrease of interregional correlation strength in juvenile mice
128 compared to infants and adults as well as age-dependent switches in correlation values among
129 several regions (Figure 2A). A Fisher r-to-z transformation test revealed several statistically
130 significant changes in interregional correlations across development (Figure S1), especially
131 between RSP, parahippocampal regions (PHR) and DORpm. Correlated activity between some
132 sets of regions changed between infant and juvenile stages and then stabilized. In other sets of

133 regions, correlated activity changed continuously from infant to adult stages, suggesting that
134 their circuits develop along a more protracted timeline.
135
136 We summarized some of the most notable changes by calculating the mean Pearson correlation
137 coefficient (r) for several combinations of regions (Figure 2B). In RSP, correlations with the
138 hippocampus and striatum were strongly negative in infants but increased in the juvenile stage
139 and then leveled off. RSP correlations with BLA parahippocampal regions were positive in
140 infants and adults but exhibited a transient decrease in juveniles. On the other hand,
141 correlations between RSP and DORpm decreased steadily from infancy to adulthood. We also
142 examined changes in correlations between DORpm regions and several cortical areas (PL, ILA,
143 ACA and RSP). In lateral (LAT), medial (MED), intralaminar (ILM) and midline (MTN) thalamic
144 nuclei, correlations with cortical areas switched from positive to negative from infancy to
145 adulthood. In anterior thalamic nuclei (ATN), correlations remained positive but decreased from
146 infant to juvenile stages and then plateaued (Figure 2B).
147
148 We next generated network graphs in which the nodes and connections represent brain regions
149 and correlations that survived thresholding using $p<0.1$ as a cutoff. In the network plots, node
150 size is proportional to degree, or the number of connections for that node (Figure 2C). Our
151 network analysis revealed that fear memory networks became sparser with age. In infants, most
152 nodes had high degrees of connectivity with all other nodes (66 edges). In juveniles, the
153 network was sparser and particular sets of regions were interconnected. For instance, subplate
154 areas including the BLA were interconnected with each other and with the hippocampal
155 formation (8/40 edges, or 20% of total connections within the network). On the other hand,
156 cortical areas were mostly connected with other cortical areas and not with the rest of the
157 regions. In adults, connectivity between cortical areas, hippocampal formation and BLA were
158 most prominent (29/50 edges, or 58% of the total connections in the network).
159
160 We calculated several measures of network tendencies to quantify changes in the organization
161 of fear memory networks across development. Network density, the ratio of the number of
162 actual links to possible links, decreased steadily from infant to adult stages. Analysis of network
163 heterogeneity revealed that networks become more clustered with age (Figure 2C). We also
164 calculated degree centrality, or the number of edges per node. Nodes in the infant network had
165 significantly more connections than in juvenile networks, but adults trended back slightly higher
166 (Figure 2D). We next computed the average shortest path length, or the number of steps along

167 the shortest paths connecting all pairs of nodes, for each age group. Nodes in adult networks
168 had significantly higher average shortest path lengths compared to both infants and juveniles
169 (Figure 2D). These results revealed significant developmental reorganization of memory
170 networks, with a shift from dense connectivity in infants to sparser more structured networks in
171 adults.
172
173 Overall, our developmental screen provided convergent evidence that a network of regions
174 known to play a key role in memory consolidation and long-term storage in adults –including
175 medial prefrontal cortex (mPFC), RSP, DORpm and PHR– is also involved in memory retrieval
176 during postnatal development. However, functional connectivity between these regions
177 reorganizes significantly between infancy and adulthood. Notably, RSP was identified in all
178 analyses in our screen (Figure 2E). RSP subregions were less activated in the infant brain
179 (Figure 1E), RSP had high salience values in our PLS analysis (Figure 1F-H), RSP was a key
180 node in memory networks at all ages (Figure 2C), and RSP underwent some of the most
181 pronounced changes in functional connectivity over development (Figure 2A,B; Figure S1).
182 While RSP has established roles in memory consolidation and long-term memory retrieval in
183 adults[34,40–43], its role in memory is poorly understood in the developing brain. Based on the
184 convergent findings in our screen, we chose to further examine the role of RSP in memory
185 retrieval and consolidation across development.
186
187 **Reactivation of TRAPed RSP neurons during memory retrieval increases with age**
188 Memory persistence has been ascribed to the reinstatement of patterns of neuronal ensemble
189 activity that were established during initial learning[44,45]. In hippocampus, mPFC and RSP,
190 neuronal ensembles that express Fos during learning or recent memory retrieval overlap with
191 Fos+ ensembles evoked during later recall[29,46]. The extent of ensemble reactivation predicts
192 retrieval success[5,26]. While RSP is known to play key roles in memory consolidation and remote
193 memory retrieval[41,47], how ensemble stability in RSP may change across development remains
194 unknown.
195
196 To determine to what extent ensembles of RSP neurons are reactivated during memory retrieval
197 across time, we used a combination of TRAP2 and immunostaining for Fos, a marker of recently
198 activated neurons (Figure 3A). Infant, juvenile or adult mice were TRAPed during 1d retrieval,
199 permanently labeling activated neurons with tdTomato. Then, following a 7d memory retrieval
200 test in the same mice, brains were collected for Fos immunostaining (Figure 3B–D). In RSP, we

201 observed no differences in the numbers of TRAPed or Fos+ cells (Figure 3E$_{1,2}$). However,
202 compared to infants and juveniles, adult mice had significantly higher levels of reactivated
203 neurons in RSP (Figure 3E$_3$). To explore the specificity of these findings, we examined
204 ensemble overlap in ACA, a neighboring cortical area that also has an established role in
205 memory consolidation and long-term storage[21,22]. In ACA, all age groups had similar numbers of
206 TRAPed, Fos+ and reactivated cells (Figure 3F$_{1–3}$). These results suggest that in the adult brain
207 RSP memory ensembles are more likely to be reactivated by salient contextual cues.
208
209 In the cortex, neurons residing in different layers (L) have distinct projection targets. L2/3
210 neurons are primarily intratelencephalic, projecting to other cortical areas, striatum and
211 subplate. L5 and L6 contain a mixture of intratelencephalic neurons, pyramidal tract neurons
212 that project to thalamus, midbrain, and spinal cord and corticothalamic neurons[48]. To gain
213 insight into whether distinct classes of projection neurons may be activated during memory
214 retrieval in different developmental stages, we calculated the number of TRAPed, Fos+ and
215 double-positive (reactivated) neurons in different cortical layers (Figure S2). In RSP, mice of all
216 ages had the most TRAPed and Fos+ neurons in L2/3 and the fewest in L6 (Figure S2A$_{1,2}$). We
217 observed significantly more reactivated cells in L2/3 for adults compared to juveniles and a
218 trend-level effect for adults vs. infants (Figure S2A$_3$). In ACA, juveniles had significantly more
219 TRAPed and Fos+ cells in L2/3 (Figure S2B$_{1,2}$) but we did not observe any layer- or age-
220 dependent differences in the distribution of reactivated neurons in ACA (Figure S2B$_3$). These
221 findings suggest that in RSP, L2/3 neurons play a prominent role in memory persistence and
222 that their likelihood of being reactivated by contextual cues increases with age.
223
224 **Reactivation of TRAPed RSP ensembles shortly after learning enhances memory in an**
225 **age-dependent manner**
226 Off-line activity within memory networks is thought to underlie memory consolidation[21]. A recent
227 study revealed that reactivation of tagged RSP memory ensembles can accelerate memory
228 consolidation[40]. We therefore hypothesized that offline reactivation of RSP memory ensembles
229 could recover lost infant memories. To test this, we injected into RSP an AAV expressing the
230 excitatory cre-dependent DREADD (designer receptor exclusively activated by designer drugs)
231 hM3Dq[49] or a control AAV that encoded a cre-dependent fluorophore. Two weeks later – when
232 mice were infants, juveniles, or adults – we performed contextual fear conditioning. The
233 following day, we TRAPed 1d memory-activated RSP neurons, thereby driving expression of
234 hM3Dq in those cells. We then performed off-line reactivation of the TRAPed ensembles by

235 administering daily the hM3Dq ligand clozapine-N-oxide (CNO, 1 mg/kg/day, intraperitoneally).
236 We administered a final dose of CNO (2 mg/kg) 30 min prior to a test retrieval session on day 7
237 (Figure 4A,B). Histology confirmed that hM3Dq-mCherry was expressed in a similar location
238 within RSP and to a similar extent across age groups (Figure S3) and that hM3Dq expressing
239 mice had significantly higher levels of activity in RSP (as assayed with Fos immunostaining)
240 compared to controls (Figure S4).
241
242 Chronic chemogenetic activation of TRAPed RSP ensembles shortly after learning affected fear
243 memory retrieval in an age-dependent manner. In infant mice, both control and hM3Dq groups
244 froze minimally during 7d retrieval, indicating that enhancing activity in RSP memory ensembles
245 in infant mice cannot prevent infantile amnesia (Figure 4C). In juveniles, control mice froze
246 slightly but significantly less during 7d vs. 1d retrieval, suggesting some fear extinction may
247 have occurred. On the other hand, juvenile hM3Dq-expressing mice froze similarly during the 1d
248 and 7d retrieval tests and significantly more than controls during 7d retrieval (Figure 4D). This
249 suggests that in juveniles, chronic reactivation of TRAPed RSP ensembles mildly enhances
250 memory. In line with previous findings[40], RSP ensemble reactivation in adult mice significantly
251 increased conditioned freezing during 7d retrieval compared to both the 1d retrieval session and
252 to 7d retrieval in control mice (Figure 4E). To further compare age-specific behaviors, we
253 computed for each hM3Dq-expressing mouse the change in freezing levels from 1d to 7d
254 retrieval (Figure 4F). All infants froze less, juveniles had no net change in freezing, and adults
255 froze more by the 7d test. Together, these data suggest that mature functions of RSP emerge
256 between juvenile and adult stages, and that memories are consolidated or retrieved via a
257 distinct mechanism in the infant brain.
258
259 To investigate the circuit-level differences underlying the distinct, age-specific effects of
260 reactivating RSP ensembles, we sacrificed the mice 60 min after the 7d retrieval test for Fos
261 immunostaining. We sectioned the brains, aligned individual slices to the Allen Brain Atlas and
262 then quantified the number of Fos+ neurons across a variety of brain regions. We focused on
263 brain regions that receive direct anatomical projects from RSP or have known functional
264 connectivity with RSP[25,35,41,50–53]. Compared to adults, infants had significantly fewer Fos+
265 neurons in the dorsal caudate putamen (CPd), several anterior thalamic nuclei (AM, AV, LD and
266 LP), and the anterior pretectal nucleus (APN), a midbrain motor nucleus (Figure 4G,H),
267 suggesting that immature functional connectivity between RSP and these regions may lead to
268 retrieval failure in infants.

Reactivation of infant-TRAPed RSP ensembles weeks after learning can recover lost memories

We next investigated whether infant-TRAPed RSP ensembles could promote memory retrieval after development had progressed. To test this, we injected into RSP an AAV encoding cre-dependent hM3Dq or a fluorophore control. Two weeks later, when mice were P17, we TRAPed RSP ensembles during contextual fear conditioning. 33d later, we delivered CNO before a memory retrieval test (Figure 5A,B). As before, histology confirmed that hM3Dq-mCherry was targeted to RSP and that hM3Dq expressing mice had significantly higher levels of activity in RSP (as assayed with Fos immunostaining) compared to controls (Figure S5).

In this experiment, hM3Dq-expressing mice froze significantly more than controls. We observed this effect in the conditioning context, but not in an altered context that had a distinct floor, wall decorations and scent (Figure 5C). Together these results reveal that infant RSP ensembles store latent memories and that once RSP cells and circuits develop, reactivating those ensembles can recover the stored infant memory. However, because activating TRAPed RSC cells only drove freezing in the conditioning context, our findings also indicate that the function of infant-TRAPed RSP ensembles are gated by the presence of salient contextual cues. Reactivating infant-TRAPed neurons in ACA or LSX did not enhance freezing 33d later (Figure S6), suggesting the effects we observed are specific to RSP.

To gain insight into which circuits may allow for recovery of lost infant memories, we then performed a week of chronic reactivation as described above in order to compare Fos downstream of infant-TRAPed RSP neurons to Fos downstream of adult-TRAPed RSP ensembles (Figure 4). We performed offline reactivation of TRAPed RSC neurons, performed another memory test on day 40 (Figure 5D), and then stained for Fos so we could compare to the findings described in Figure 4. We found that after allowing development to progress for 33d, reactivation of infant-TRAPed RSP ensembles largely recapitulated the Fos activation patterns we observed in adults (Figure 5E). There were two exceptions in the regions analyzed – AD and AM, suggesting that enhancement of activity in other regions (CPd, APN, LD, LP) may be responsible for the recovery of conditioned freezing.

Discussion

302 Even though very early experiences cannot be explicitly recalled, they can profoundly impact
303 the rest of our life[5,7,54]. Recent work shed light on this paradox, showing that infant memories
304 are not erased but rather inaccessible[11,13,15–17]. But why infant memories become inaccessible
305 was poorly understood. We hypothesized that one of two potential models may be at play. In the
306 first, distinct circuits store memories early in development and are no longer used in adulthood.
307 In the second, the same circuits are involved but function in different ways over development.
308 To investigate this, we designed a brain-wide screen to identify developmental changes in
309 memory retrieval circuits. Evidence from our developmental screen supported the second
310 model. We found that while similar brain regions encode memory throughout development,
311 changes in their behavioral functions and network organization align with the emergence of
312 persistent memory.
313
314 Our focused analyses revealed that RSP functional maturation aligns with the emergence of
315 persistent memories. RSP had more activated cells during memory retrieval in adults compared
316 to juveniles and infants. RSP functional connectivity with association cortices, hippocampus,
317 and amygdala - all key regions for memory encoding, consolidation and retrieval - changed
318 significantly across development. We defined the time course of RSP functional maturation,
319 showing that RSP memory ensembles were more likely to be reactivated by salient contextual
320 cues in adults compared to juveniles and infants (Figure 6). Along the same lines, reactivating
321 TRAPed RSP ensembles at 7 days enhanced memory in adults but not in infant mice and had
322 an intermediate effect in juveniles. But when we TRAPed RSP ensembles in infancy and then
323 allowed development to progress, reactivating TRAPed RSP ensembles after 30d successfully
324 recovered lost infant memories. This effect was only present in the conditioning context and not
325 in a modified context with distinct sensory cues. These findings indicate that in infancy,
326 memories are consolidated or retrieved through distinct mechanisms compared to adults due to
327 an immature RSP. Furthermore, our data indicate that while learning-activated RSP ensembles
328 encode latent infant memories over time, salient sensory cues do not activate those original
329 cells, so retrieval does not occur.
330
331 Our work extends models of infantile amnesia to include a key role for the retrosplenial cortex.
332 Current models center on hippocampal maturation. In infants, learning promotes hippocampal
333 synaptic maturation via signaling pathways that are involved in critical periods in other brain
334 regions, suggesting that the infant hippocampus is in a critical period for learning systems.[13]
335 These studies led the authors to propose the retrieval hypothesis, in which an immature

336 hippocampus stores information in a latent form such that it fails to be retrieved without
337 extensive reminders. In this model, learning promotes hippocampal maturation and drives
338 transitions through sequential critical periods. In each critical period, the hippocampus becomes
339 better at storing information such that it can be actively retrieved later[14]. Other studies showed
340 that in the infant brain, naturally high levels of hippocampal neurogenesis promote forgetting but
341 infant memories are stored in a dormant state in hippocampal ensembles[9,11]. This led the
342 authors to propose a (non-mutually exclusive) neurogenic hypothesis of infantile amnesia, in
343 which neurogenesis-induced circuit remodeling underlies infantile amnesia[5,55].
344
345 Our findings build upon this work, suggesting that the immature RSP contributes to the retrieval
346 failure of infant memories. Our data suggest that in infancy, an immature RSP can store
347 memories but cannot retrieve them due to immature functional connectivity with
348 parahippocampal and thalamic regions. Previous studies showed that offline reactivation of
349 tagged RSP ensembles accelerates memory consolidation in adults[40]. In our developmental
350 studies of RSP functions, we activated TRAPed neurons offline and immediately before memory
351 retrieval. So, we cannot distinguish the role of RSP in memory consolidation vs. retrieval. Still,
352 our results suggest that while activating TRAPed RSP enhances memory in adults, these
353 functions are absent in infants and only begin to emerge in juveniles. We also found that infant-
354 tagged RSP ensembles are less likely to be reactivated by salient contextual cues as compared
355 to adults. Furthermore, chemogenetically reactivating infant-TRAPed RSP neurons 33d later
356 enhanced freezing, but only in the conditioning context. This suggests that neither conditioned
357 sensory cues nor chemogenetic activation of RSP ensembles are alone sufficient to evoke
358 freezing behavior, but that they can do so in combination. In infants, immature RSP functional
359 connectivity and weak activation of RSP ensembles by conditioned stimuli may contribute to the
360 inability to retrieve infant memories. During development, these processes may be linked or
361 may be independently at play.
362
363 It remains to be determined how an immature hippocampus may influence the ability of the
364 infant RSP to encode, consolidate and retrieve memories. RSP serves as an input structure to
365 the hippocampus, providing important spatial cues. RSP also serves as a target of hippocampal
366 output during systems consolidation[56]. In adults, transfer of information from the hippocampus to
367 RSP is critical for the formation of long-term memories in the RSP[57–59] and for subsequent
368 memory retrieval[56,60,61]. In infants, the immature hippocampus could lead to weaker memory
369 representations in RSP as compared to adults. But we show that directly stimulating infant-

370 TRAPed RSP ensembles can recover the infant memory, suggesting that some post-learning
371 hippocampal-RSP information transfer has taken place. Further, our analyses indicate that in
372 infants, weaker functional connectivity between RSP and anterior thalamic nuclei and midbrain
373 motor areas may underlie retrieval failure. Future studies can examine how RSP connections
374 with the hippocampus, anterior thalamic nuclei and midbrain influence developmental transitions
375 in memory persistence.
376
377 The neural mechanisms of memory retrieval are well studied in adults but remain poorly
378 understood in the developing brain. Our studies provide novel insights into the organization of
379 fear memory networks in the developing brain and point to RSP as a key player in the
380 maturation of memory. Our whole brain analyses revealed that during recent memory retrieval
381 (1d after learning), similar sets of regions underlie conditioned freezing (Figure 2). These
382 included RSP, ACA, motor and sensory cortices, lateral hypothalamus, and midbrain. RSP was
383 a key node in recent (1d) fear memory networks at each age examined, but these networks had
384 distinct organization (Figure 3). Juvenile networks were sparser than in infants and adults. In
385 infants, most network nodes were interconnected, while adult networks had more structure, with
386 notable connections between RSP, frontal association areas, parahippocampal regions and
387 BLA. Even though juveniles and adults had similar freezing levels across time, distinct circuit
388 architectures underlie fear memory retrieval in these two age groups. This suggests that juvenile
389 and adult fear memories likely have unique mechanisms of consolidation, storage and retrieval.
390
391 In adults, in both rodents and humans, RSP plays a key role in learning[42,62,63], consolidation[64,65]
392 and recent and remote memory retrieval[61,66–68], but how and when RSP functionally matures
393 was largely unknown. We showed that infant RSP ensembles active during fear conditioning
394 encoded long-term memories but were not reactivated by contextual cues. We also found that
395 offline reactivation of RSP ensembles can promote memory retrieval beginning in juvenile
396 stages and these functions are further enhanced in adults. Together with the whole brain
397 analyses of TRAPed cells, these studies indicate that RSP is involved in learning and recent
398 memory retrieval beginning in infancy and plays an increasing role in memory consolidation and
399 long-term memory retrieval between juvenile and adult stages.
400
401 Our studies provide novel insights into the RSP circuit mechanisms underlying memory retrieval
402 and consolidation in adults and align maturation of RSP functional connectivity with its changing
403 role in memory. RSP is densely interconnected with sensory cortices, with limbic regions that

404 are important for memory encoding, and with anterior thalamic nuclei and cortical regions
405 important for long-term memory storage and retrieval[21,57,69–79]. In developing rats, bidirectional
406 connections linking RSP to the hippocampal formation reach adult-like densities by P12[25,26]. In
407 humans, resting state functional connectivity between RSP and the prefrontal cortex increases
408 between adolescence and early adulthood while RSP-hippocampal functional connectivity
409 matures earlier[80]. But little is known about how and when RSP circuits underlying memory
410 retrieval functionally mature.
411
412 We show that activating RSP in the conditioning context led to age-specific patterns of Fos
413 induction in downstream regions. Infants had fewer Fos+ cells in anterior thalamic nuclei, dorsal
414 striatum and midbrain motor nuclei. Because we did not observe differences in the layer
415 distribution of TRAPed cells (Figure S2), it is unlikely that the distinct patterns of Fos arose from
416 TRAPing different classes of projection neurons at each age. Instead, immature connectivity
417 with striatum, anterior thalamic nuclei and midbrain areas may influence the ability to
418 consolidate or retrieve memories, leading to retrieval failure in infants. Reactivating infant
419 TRAPed RSP neurons one month after training was sufficient to induce freezing behavior, but
420 only in the conditioning context, indicating that RSP ensemble function is gated by salient
421 sensory cues. Memory retrieval is thought to involve brain-wide reinstantiation of patterns of
422 activity established during learning, but in the cortex, synaptic connections remodel until early
423 adulthood. Consistent with previous work that suggests hippocampal circuit remodeling
424 promotes forgetting[55], our studies indicate that during development, synaptic remodeling within
425 infant RSP memory-encoding ensembles may diminish the likelihood of instantiating original
426 patterns of ensemble activity. This could break the links between salient sensory stimuli and
427 conditioned behaviors, leading to retrieval failure.
428
429 Early life adversity like chronic stress is a major risk factor for developing mental health
430 disorders. Early adversity can lead to premature emergence of persistent memories, suggesting
431 that accelerated development of memory systems may be linked to poor mental health
432 outcomes[7,18–20]. In aging models of neurodegeneration, in which subjects display a similar level
433 of forgetting as in infantile amnesia, memory impairment corresponds to the degeneration of
434 memory circuits that include the RSP[81,82]. By illustrating how memory retrieval networks change
435 across development, our work builds a foundation for understanding how adverse rearing
436 conditions may influence neurodevelopmental trajectories, leading to problematic behaviors in
437 adulthood. Further, revealing the organization and function of memory networks in animals with

438 infantile amnesia may provide mechanistic insight into memory disorders associated with
439 forgetting[83].
440

441 ## Acknowledgments

442 We thank Carlos Portera-Cailliau and Scott Wilke for feedback on the manuscript. This
443 publication was supported by a NARSAD Young Investigator Award from BBRF (L.A.D.),
444 Whitehall Foundation Grant (L.A.D.), Klingenstein-Simons Fellowship in Neuroscience (L.A.D.),
445 R01MH127214 (L.A.D), T32 MH073526 (B.J.), Jessamine Hilliard Neurobiology Graduate
446 Student Grant Program (B.J) and UCLA Dissertation Year Fellowship (B.J.). Confocal imaging
447 was performed in the UCLA Broad Center for Regenerative Medicine and Stem Cell Research
448 microscopy core. Figure 6 was produced using BioRender.com.

449 ## Author Contributions

450 Conception, B.J. and L.A.D.; Methodology, B.J., M.W.G., L.O., L.H.W., B.W., A.D., Y.N.
451 S.A.R.M., and L.A.D.; Investigation, B.J., ; Writing – Original Draft, B.J. and L.A.D.; Writing –
452 Review & Editing, B.J., M.W.G., L.A.D.; Funding Acquisition, B.J. and L.A.D.

453 ## Declaration of Interests

454 The authors declare no competing financial interests.

455 ## Figure Titles & Legends

456 **Figure 1. A developmental screen to identify neural signatures of infantile amnesia.**
457 (A) Infant, juvenile, and adult mice underwent contextual fear conditioning and then memory
458 testing 1 or 7 days later.
459 (B) Percent time freezing in infant, juvenile and adult wildtype mice during memory retrieval
460 tests occurring 1 or 7 days after CFC ($F_{age}(2,45)=15.89$, $P<0.0001$, $F_{day}(1,45)=3.56$, $P=0.07$,
461 $F_{int}(2,45)=4.21$, $P=0.02$, Infant: N=7 1d, N=10 7d; Juvenile: N=14 1d, N=8 7d; Adult: N=7 1d,
462 N=6 7d, two-way ANOVA with Tukey post-hoc test).
463 (C_1) Experimental design for developmental screen.
464 (C_2) Freezing behavior in TRAP mice used in screen ($F(2,22)=1.87$, $P=0.18$, One way ANOVA;
465 N=7 infant, N=9 juvenile, N=9 adult).
466 (D) Representative 100-μm thick optical z-stacks showing TRAPed cells from 1-day retrieval.

467 (E) TRAPed cell counts by age (Sensory cortex: $F_{region}(2.03,44.7)=267.30$, $P<0.0001$;
468 $F_{age}(2,22)=0.02$, $P=0.97$; $F_{int}(10,110)=0.65$, $P=0.77$; Association cortex:
469 $F_{region}(3.45,75.93)=132.7$, $P<0.0001$; $F_{age}(2,22)=3.82$, $P=0.38$; $F_{int}(24,264)=2.14$, $P=0.002$;
470 Sensory Thalamus: $F_{region}(1.18,26.04)=80.39$, $P<0.0001$; $F_{age}(2,22)=0.69$, $P=0.51$;
471 $F_{int}(10,110)=1.05$, $P=0.41$; Polymodal thalamus: $F_{region}(2.22,48.84)=28.77$, $P<0.0001$;
472 $F_{age}(2,22)=7.60$, $P=0.003$; $F_{int}(12,132)=1.59$, $P=0.10$; Hypothalamus/Midbrain:
473 $F_{region}(3.38,74.38)=141.0$, $P<0.0001$; $F_{age}(2,22)=3.10$, $P=0.07$; $F_{int}(10,110)=2.61$, $P=0.007$;
474 Subplate: $F_{region}(2.96,65.07)=149.7$, $P<0.0001$; $F_{age}(2,22)=1.93$, $P=0.17$; $F_{int}(12,132)=1.42$,
475 $P=0.17$; Hippocampal Formation: $F_{region}(1.94,42.58)=43.78$, $P<0.0001$; $F_{age}(2,22)=2.16$, $P=0.14$;
476 $F_{int}(24,264)=0.82$, $P=0.72$. Infant N=7, Juvenile N=9, Adult N=9; Two-way repeated measure
477 ANOVAs with Tukey post-hoc correction test).
478 (F-H) Task PLS analysis of TRAPed cell densities in (F) infants, (G) juveniles and (H) adults.
479 Dashed lines indicate threshold of 3. Color labels on x-axis correspond to major brain
480 subdivisions according to the Allen Brain Atlas.
481 See Tables S1 and S2 for abbreviations and statistics. Graphs show mean $\pm$ SEM. *P< 0.05,
482 **P<0.01, ***P<0.001. Scale bars, 100 μm.
483
484 **Figure 2. Developmental changes in fear memory networks.**
485 (A) Pearson correlation matrices showing interregional correlations based on numbers of
486 TRAPed cells at 1-day memory retrieval across ages. Colors reflect Pearson correlation
487 coefficients (scale, right) and labels within squares correspond to p values from pairwise
488 comparisons.
489 (B) Mean pearson r values for left: RSP ($F_{region}(4,48) = 12.47$, $P<0.0001$; $F_{age}(2,48) = 1.04$,
490 $P=0.37$; $F_{interaction}(8,48) = 5.60$, $P<0.0001$; HPF: N=3; STR: N=4; BLA: N=3; PHR: N=6; TH: N=5
491 brain regions) and right: between dorsal cortex (PL, ILA, ACA, RSP) and dorsal polymodal
492 thalamic nuclei (DORpm, $F_{region}(4, 45) = 5.82$, $P=0.0007$; $F_{age}(2, 45) = 26.48$, $P<0.0001$;
493 $F_{interaction}(8, 45) = 1.36$, $P=0.24$; N=4 cortical brain regions). Two-way ANOVAs with Tukey post-
494 hoc correction test.
495 (C) Network graphs generated for Pearson's correlations p<0.1 Regions are grouped and
496 colored according to major brain subdivision as defined by the Allen Brain Atlas. The node size
497 is proportional to the number of connections (degree) and the weights of the lines are
498 proportional to the correlation strength.

499 (D) Average degree (left, $F(2,75)=5.21$, $P=0.008$, One-way ANOVA) and shortest path length
500 (right, $F(2,75)=18.34$, $P<0.0001$, One-way ANOVA) for each network node for each age (Infant:
501 N=24; Juvenile: N=28; Adult: N=26 nodes).
502 (E) Summary of convergent findings from analyses presented in Figures 1 and 2.
503 *P< 0.05, **P<0.01, ***P<0.001, ****P<0.0001. Graphs show mean ± SEM. See also Figure S1
504 for additional network analyses.
505
506 **Figure 3. Selectively increased reactivation of memory-encoding ensembles in RSP in**
507 **adults.**
508 (A) Illustration of stable vs. dynamic ensembles in a TRAP/Fos overlay assay.
509 (B) Experiment design for activity-dependent tagging of ensembles between 1- and 7-day
510 retrieval.
511 (C) Illustration of analysis sites for RSP and ACA.
512 (D) Representative examples of TRAPed (magenta) and Fos+ cells (green) in the anterior
513 cingulate (top) and retrosplenial cortices (anterior, middle; posterior, bottom).
514 (E_1) TRAPed cells per ROI for ACA ($F(2,16)=0.34$, $P=0.72$, one-way ANOVA with Tukey post-
515 hoc correction; Infant: N=4, Juvenile: N=8, Adult: N=7).
516 (E_2) Fos+ cells per ROI for ACA each region and age group ($F(2,16)=2.11$, $P=0.15$, one-way
517 ANOVA with Tukey post-hoc correction; Infant: N=4, Juvenile: N=8, Adult: N=7).
518 (E_3) Double-labeled neurons per ROI for ACA ($F(2,16)=0.39$, $P=0.68$, one-way ANOVA with
519 Tukey post-hoc correction; Infant: N=4, Juvenile: N=8, Adult: N=7).
520 (F_1) TRAPed cells per ROI for RSP ($F(2,11)=0.09$, $P=0.92$, one-way ANOVA with Tukey post-
521 hoc correction; Infant: N=4, Juvenile: N=5, Adult: N=5).
522 (F_2) Fos+ cells per ROI for RSP each region and age group ($F(2,11)=0.70$, $P=0.52$, one-way
523 ANOVA with Tukey post-hoc correction; Infant: N=4, Juvenile: N=5, Adult: N=5).
524 (F_3) Double-labeled neurons per ROI for RSP ($F(2,11)=7.1$, $P=0.01$, one-way ANOVA with
525 Tukey post-hoc correction; Infant: N=4, Juvenile: N=5, Adult: N=5).
526 Graphs show mean ± SEM. *P <0.05. See also Figure S2 for layer analysis.
527
528 **Figure 4. Chemogenetic reactivation of TRAPed RSC neurons increased freezing during**
529 **short-term memory retrieval in an age-dependent manner.**
530 (A) Experimental design.
531 (B) Representative coronal section showing AAV injection site in RSP. Scale bar, 125 μm.

532 (C) Percent freezing levels at 1- and 7-day retrieval in control (grey) and hM3Dq (brown) groups
533 for infants ($F_{virus}(1,7)=1.29$, $P=0.29$, $F_{day}=(1,7)=24.18$, $P=0.002$; $F_{int}(1,7)=0.47$, $P=0.51$, Cont:
534 N=4, hM3Dq: N=5, two-way ANOVA with Holm-Sidak post hoc test).
535 (D) Percent freezing levels at 1- and 7-day retrieval in control (grey) and hM3Dq (magenta)
536 groups for juveniles ($F_{virus}(1,28)=1.81$, $P=0.19$, $F_{day}=(1,7)=3.33$, $P=0.07$; $F_{int}(1,7)=4.34$, $P=0.04$,
537 Cont: N=16, hM3Dq: N=14, two-way ANOVA with Holm-Sidak post hoc test).
538 (E) Percent freezing levels at 1- and 7-day retrieval in control (grey) and hM3Dq (teal) groups
539 for adults ($F_{virus}(1,28)=1.81$, $P=0.19$, $F_{day}=(1,7)=3.33$, $P=0.07$; $F_{int}(1,7)=4.34$, $P=0.04$, Cont: N=8,
540 hM3Dq: N=10, two-way ANOVA with Holm-Sidak post hoc test).
541 (F) Differences in freezing levels between 7-day and 1-day retrieval sessions for hM3Dq mice in
542 each age group ($F(2,26)=12.92$, $P=0.001$, Infant: N=5, Juvenile: N=14, Adult: N=10, one-way
543 ANOVA with Tukey post hoc test).
544 (G) Representative images showing Fos immunoreactive cells in dorsal caudate putamen
545 (CPd), anteromedial thalamus (AM), laterodorsal thalamus (LD), and anterior pretectal nucleus
546 (APN). Scale bars, 100 μm.
547 (H) Quantification of Fos+ cells per ROI in 19 brain regions ($F_{region}(18,160)=30.03$, $P<0.05$;
548 $F_{age}(2,9)=3.69$, $P>0.05$; $F_{int}(36,160)=5.78$, $P<0.05$, Mixed Effects Model; Infant: N=4; Juvenile:
549 N=4; Adult: N=3-4).
550 Graphs show mean ± SEM. * P<0.05, **P<0.01, ***P<0.001, ****P<0.0001. See also Figure S3
551 and S4.
552
553 **Figure 5. Chemogenetic reactivation of learning encoding ensembles in RSC 33d after**
554 **training recovers infant memories**
555 (A) Experimental design.
556 (B) Representative coronal section showing AAV injection site in RSP. Scale bar, 125 μm.
557 (C) Percent freezing levels in contexts A and B during the 33-day retrieval test in control (gray)
558 and hM3Dq (brown) mice ($F_{virus}(1,14)=9.06$, $P=0.009$; $F_{context}(1,14)=7.41$, $P=0.01$;
559 $F_{int}(1,14)=5.23$, $P=0.03$, Cont: N=8, hM3Dq: N=8, two-way ANOVA with Holm-Sidak posthoc
560 test).
561 (D) Percent freezing levels in contexts A and B during the 40-day retrieval test in control (gray)
562 and hM3Dq (brown) mice ($F_{virus}(1,14)=9.81$, $P=0.007$; $F_{context}(1,14)=12.3$, $P=0.003$;
563 $F_{int}(1,14)=4.65$, $P=0.07$, Cont: N=8, hM3Dq: N=8, two-way ANOVA with Holm-Sidak posthoc
564 test).

565 (E) Comparison of regional Fos levels in P17-TRAP+40d vs. Adult TRAP from Figure 4
566 ($F_{region}(18,121)=18.97$, $P<0.0001$; $F_{age}(1,7)=3.05$, $P=0.12$; $F_{int}(18,121)=3.5$, $P<0.0001$, Inf: N=5,
567 Adult: N=4, two-way mixed effects repeated measures analysis with Sidak posthoc test).
568 Graphs show mean ± SEM. *P<0.05. See also Figures S5 and S6.

569 STAR Methods

570 **Resource availability**

571

572 Further information and request for resources and reagents should be directed to and will be
573 fulfilled by the lead contact, Laura A. DeNardo (ldenardo@ucla.edu)

574

575 **Materials availability**

576 This study did not generate new unique reagents.

577

578 **Data and code availability**

579 Whole brain TRAP data are presented in Table 2 and previously published code for
580 DeepCOUNT can be found in the DeNardo lab GitHub database
581 (https://github.com/DeNardoLab). Any additional information required to reanalyze the data
582 reported in this paper is available from the lead contact upon request.

583 **Experimental model and study participant details**

584 **Animals**

585 Female and male C57B16/J mice (JAX Stock No. 000664) or TRAP2;Ai14 mice (JAX Stock
586 Nos. 030323 and 007914) were group housed (2–5 per cage) and kept on a 12 hour light cycle
587 (lights on 7am-7pm). All animal procedures followed animal care guidelines approved by the
588 University of California, Los Angeles Chancellor's Animal Research Committee.

589 **Method Details**

590

591 **Surgery**

592 Animals underwent surgery at P3, P9 or P46. Depending on the experiment, mice were
593 anesthetized through hypothermia (P3 mice), or induced in 5% isoflurane in oxygen until loss of
594 righting reflex (P9 or older) and transferred to a stereotaxic apparatus with rubber ear bars. P9+

595 mice were maintained under 2% isoflurane in oxygen, and warmed with a circulating water
596 heating pad throughout surgery and eye gel was applied to the animal's eyes. The mouse's
597 head was shaved and prepped with three scrubs of alternating betadine and then 70% ethanol.
598 Following a small skin incision, a dental drill was used to drill through the skulls above the
599 injection targets. A syringe pump (Kopf, 693A) with a Hamilton syringe was used for injections
600 delivered at a rate 100nL/min. The syringe was left in the brain for 1 or 7 minutes (min) following
601 injection for P3 and P9+ mice respectively. For DREADD studies, a small volume of AAV8-
602 hSyn-DIO-hM3D(Gq)-mCherry virus (Addgene 44361, final titer 2 x 10^{12} pp per mL) was
603 injected bilaterally into RSC (AP: -2.7, ML: $\pm$ 0.3, DV: 1.0). At P3 and P9, this coordinate was
604 scaled using Neurostar StereoDrive software (Neurostar) which corrects for head size,
605 orientation, and tilt. To compensate for age-dependent changes in cortical volume, we made
606 proportional adjustments to the volume of injected virus based on previous developmental
607 studies[84]: 0.15 µL for P3, 0.2 µL for P9, and 0.4 µL for P46 mice. Control mice received
608 injections of age-matched volumes of AAV1-pCAG-FLEX-eGFP-WPRE (Addgene 51502, final
609 titer 1 x 10^{13} pp per mL) into RSC. For pain management mice received 5 mg/kg carprofen
610 diluted in 0.9% saline subcutaneously. Mice received one carprofen injection 30 min prior to
611 surgery and daily injections for two days following surgery. Following confirmatory histology,
612 samples with mistargeted injection sites were excluded from analysis.
613
614 **4-Hydroxytamoxifen Preparation**
615 4-hydroxytamoxifen (4-OHT; Sigma, Cat# H6278) was dissolved at 20 mg/mL in ethanol by
616 shaking at 37°C for 15 min and was then aliquoted and stored at –20°C for up to several weeks.
617 Before use, 4-OHT was redissolved in ethanol by shaking at 37°C for 15 min, a 1:4 mixture of
618 castor oil:sunflower seed oil (Sigma, Cat #s 259853 and S5007) was added to give a final
619 concentration of 10 mg/mL 4-OHT, and the ethanol was evaporated by vacuum under
620 centrifugation. The final 10 mg/mL 4-OHT solutions were always used on the day they were
621 prepared. All injections were delivered intraperitoneally (i.p.).
622
623 **Behavioral assays**
624 Mice were placed in an operant chamber with a shock floor. They received 5 1 second, 0.5 mA
625 foot shocks separated by 1 min. On retrieval days, mice were placed in the conditioning
626 chamber for 5 min. For TRAP experiments, mice were injected with 4-OHT solution immediately
627 following the retrieval session. Point-tracking of behavioral videos was performed in
628 DeepLabCut[85]. Locomotion and freezing behavior was analyzed using BehaviorDEPOT[86].

629

630 **Brain Clearing**

631 Two weeks after TRAPing, mouse brains were collected and processed based on the published
632 Adipo-Clear protocol[32] with slight modifications. Mice were perfused intracardially with 20mL of
633 PBS (Gibco) followed by 4% paraformaldehyde (PFA, Electron Microscopy Sciences) on ice.
634 Brains were hemisected approximately 1 mm past midline and postfixed overnight in 4% PFA at
635 4°C. The following day, samples were dehydrated with a gradient of methanol (MeOH, Fisher
636 Scientific):B1n buffer (1:1,000 Triton X-100, 2% w/v glycine, 1:10,000 NaOH 10N, 0.02%
637 sodium azide) for 1 hour for each step (20%, 40%, 60%, 80%) on a nutator (VWR). Samples
638 were then washed with 100% MeOH 2x for 1 hour each and then incubated in a 2:1
639 dicholoromethane (DCM):MeOH solution overnight. The following day, two washes of 1 hour in
640 100% DCM were performed followed by three washes of 100% MeOH for 30 min, 45 min then 1
641 hour. Samples were bleached for 4 hours in 5:1 H2O2/MeOH buffer. A cascade of MeOH/B1n
642 washes (80%, 60%, 40%, 20%) for 30 min each rehydrated the samples followed by a 1 hour
643 wash in B1n buffer. 5%DMSO/0.3M Glycine/PTxWH permeabilized tissue for one hour and then
644 again for 2 hour with fresh solution. Samples were washed with PTxwH for 30 min and then
645 incubated in fresh PTxwH overnight. The following day two more PTxwH washes lasted 1 hour
646 then 2 hours. For TRAP2 experiments, samples were incubated in primary RFP antibody
647 (Rockland 600-401-379) at 1:300 in PTxwH shaking at 37°C for 11 days, washed in PTxwH 2x1
648 hour and then 2x2 hours, then for two days with at least one PTxwH change per day while
649 shaken at 37°C. Samples were then incubated in secondary antibody AlexaFluor 647, catalog
650 #A-31573, 1:300, ThermoFisher Scientific) for 8 days shaken at 37°C. Samples were washed in
651 PTxwH 2x1 hour, then 2x2 hour, then 2 days with at least one PTxwH change per day while
652 shaken at 37°C. Samples were then washed in 1x PBS twice 1x1 hour, 2x2 hours and then
653 overnight. To dehydrate samples, a gradient of washes in MeOH:H2O (20%, 40%, 60% and
654 80%) were conducted for 30 min each, followed by 3x100% MeOH for 30 min, 1 hour, then 1.5
655 hours. Samples were incubated overnight in 2:1 DCM:MeOH on a nutator. The next day,
656 samples were washed in 100% DCM 2x1 hour each. Samples were then cleared in 100%
657 dibenzyl ether (DBE). DBE was changed after 4 hours. Samples were stored in DBE in a dark
658 place at room temperature. Imaging took place at least 24 hours after clearing. Samples with
659 poor antibody penetration following tissue clearing were excluded from analysis.

660

661 **Whole Brain Imaging**

662 Brain samples were imaged on a light-sheet microscope (Ultramicroscope II, LaVision Biotec)
663 equipped with a sCMOS camera (Andor Neo) and a 2x/0.5 NA objective lens (MVPLAPO 2x)
664 equipped with a 6 mm working distance dipping cap. Image stacks were acquired at 0.8x optical
665 zoom using Imspector Microscope v285 controller software. For TRAP2;Ai14 brains, we imaged
666 using 488-nm (laser power 20%) and 640-nm (laser power 50%) lasers. The samples were
667 scanned with a step-size of 3 µm using the continuous light-sheet scanning method with the
668 included contrast adaptive algorithm for the 640-nm channel (20 acquisitions per plane), and
669 without horizontal scanning for the 488-nm channel.
670
671 **DeepCOUNT Analysis**
672
673 ***Image Registration & Cell Segmentation***
674 Whole-brain TRAP counts were obtained using DeepCOUNT as previously described[30]. Briefly,
675 whole-brain image stacks from the 640nm channel from each brain were segmented in
676 TrailMap[87] using the TRAP2-Ai14 trained model. Images were registered to the template brain
677 using elastix and transformix using the 488nm autofluorescence channel. MATLAB was used to
678 identify 3D maxima of the transformed probability map. Connected component analysis was
679 used to reduce any maxima that consisted of multiple pixels into a single pixel per cell.
680
681 ***Cell Quantification***
682 Regional TRAPed cell density was quantified in MATLAB (Mathworks) by counting the number
683 of labeled pixels (i.e. cells) in each brain region, then dividing this pixel count by the total
684 number of pixels in a region. This regional pixel count was then divided by the total number of
685 detected cells across the brain to normalize for differences in tamoxifen-induced recombination.
686 Regions were defined by a collapsed version of the LSFM atlas in which maximum granularity
687 was balanced with the need to account for slight differences in registration which would lead to
688 inaccurate quantification of small brain regions. This atlas was cropped on the anterior and
689 posterior ends to match the amount of tissue visible in our data. Fiber tracts, ventricular
690 systems, cerebellum, and olfactory bulb were excluded from analysis. For comparison of
691 regional TRAPed counts between ages, Two-way repeated measures ANOVA with post-hoc
692 multiple comparison correction was performed to identify statistically significant differences
693 between brain regions. All statistical comparisons were performed in GraphPad Prism v10.
694
695 **Functional Network Construction**

696 In MATLAB, we calculated simple linear correlations between all pairs of brain regions based on
697 the normalized, per area TRAPed cell counts. The nodes and connections in the networks
698 represent brain regions and correlations that survived thresholding using $P<0.1$ as a cutoff.
699 While potentially interesting, we did not consider negative correlations in the current analysis.
700 We used Cytoscape software to visualize and analyze networks. Degree was calculated by
701 counting all the above-threshold connections for a given node. Node size is proportional to
702 degree and lines represent above-threshold correlations.
703
704 **Brain Slice Histology and Immunostaining**
705 Mice were transcardially perfused with phosphate-buffered saline (PBS) followed by 4%
706 paraformaldehyde (PFA) in PBS. Brains were dissected, post-fixed in 4% PFA for 12–24 hours
707 and placed in 30% sucrose for 24–48 hours. They were then embedded in Optimum Cutting
708 Temperature (OCT, Tissue Tek) and stored at -80°C until sectioning. 60 µm floating sections
709 were collected into PBS. Sections were washed 3x10 min in PBS and then blocked in 0.3%
710 PBST containing 10% normal donkey serum (catalog #17-000-121, Jackson Immunoresearch)
711 for 2 hours. Sections were then incubated in a carrier solution (3% donkey serum in 0.3%
712 PBST) containing the primary antibodies for two nights at 4°C. Two days later, sections were
713 washed 3x5 min in PBS and then stained in a carrier solution (5% donkey serum in 0.3% PBST)
714 with secondary antibody for 2 h at room temperature. The following primary antibodies were
715 used: polyclonal chicken anti-GFP (catalog #1020, 1:2000, Aves), monoclonal rabbit anti-RFP
716 (catalog #600-401-379, 1:2000, Rockland), monoclonal rabbit anti-Fos (catalog #226-008,
717 1:2000, Synaptic Systems) , and mCherry monoclonal anti-rat (catalog #M11217, 1:500,
718 ThermoFisher). The following secondaries were used: Cy2 polyclonal donkey anti-chicken
719 (catalog #703-225-155, 1:1000, Jackson Immunoresearch), Cy3 polyclonal donkey anti-rabbit
720 (catalog #711-005-152, 1:1000, Jackson Immunoresearch), Alexa647 polyclonal donkey anti-
721 rabbit (catalog #711-605-152, 1:1000, Jackson Immunoresearch), and Cy3 polyclonal donkey
722 anti-rat (catalog #712-165-153, 1:1000, Jackson Immunoresearch). Sections were then washed
723 5 min with PBS, 15 min with PBS+DAPI (catalog #D1306, 1:4000, Thermofisher), and then 5
724 min with PBS. Sections were mounted on glass slides using FluoroMount-G (catalog #00-4958-
725 02, ThermoFisher) and then imaged at 10x with a Zeiss 700 confocal microscope or at 10x on a
726 Leica DM6 B scanning microscope.
727
728 **DREADD Studies**

729 To activate neurons, we used a cre-dependent virus expressing the excitatory DREADD (pAAV-
730 hSyn-DIO-hM3D(Gq)-mCherry) or a fluorophore control (pAAV-hSyn-DIO-mCherry) in TRAP2
731 mice two weeks prior to fear-conditioning. Viral expression was driven exogenously by
732 intraperitoneally delivered 4-hydroxytamoxifen, which induced fos-dependent expression of cre-
733 recombinase in the TRAP2 mice, allowing specific tagging and long-term labeling of memory
734 encoding ensembles for weeks later. To determine the effects of chronic activation of TRAPed
735 RSC ensembles during development (i.e. comparing freezing levels between retrieval days 1
736 and 7), 4-hydroxytamoxifen was intraperitoneally injected immediately after 1-day retrieval to tag
737 ensembles involved in retrieval and consolidation (Figure 4) or immediately after contextual fear
738 conditioning (Figure 5).
739
740 30 min prior to their first retrieval session, mice were intraperitoneally injected with CNO
741 dissolved in 0.9% saline (1mg/kg, i.p., Fisher Scientific). After the first retrieval session, mice
742 were returned to their home cage. A subset of mice were also tested in an alternate context 3
743 hours after the first testing session, and then returned to their home cage. Following the first
744 retrieval test, mice were injected daily with CNO (2 mg/kg, i.p.) for 5 days and then returned to
745 the homecage. 30 min prior to the last retrieval day, CNO (1 mg/kg, i.p.) was injected prior to
746 testing in a similar manner as the first retrieval day. Mice were perfused 1 hour after the last
747 retrieval session and their brains collected and processed for Fos immunostaining.
748

749 **Fos Analysis in 2-D sections**

750 ***Alignment***

751 Following Fos immunostaining and imaging as described above, sections were aligned to the
752 Allen Brain Atlas[88] using DeepSlice[89], a deep-learning based algorithm for automatically
753 calculating the position and slicing angle of each section in relation to the atlas. The DAPI
754 channel was used for alignment. Alignments were imported to the ABBA plugin for FIJI[90,91]
755 (https://biop.github.io/ijp-imagetoatlas/) which was used to manually check the alignment for
756 each section. ROIs from ABBA were then exported to FIJI, and ROIs for regions to be analyzed
757 were manually checked for tissue damage and image quality.

758 ***Fos$^+$ Cell Detection***

759 Images of the Fos channel were processed using a custom deep learning pipeline. This pipeline
760 has largely the same architecture as our existing 3D pipeline, DeepCOUNT[30], but uses a 2D U-

761 Net instead of a 3D U-Net. A network for segmenting Fos^+ cells was trained and validated using
762 manually annotated 100x100 pixel images. Following model training, each section was
763 segmented for Fos^+ cells. Cells were quantified using 2D maxima detection on the segmented
764 images in FIJI. The number of detected cells in each region was divided by the area of that
765 region to generate Fos density counts.

766

767 **Quantification and Statistical Analysis**

768 Results were plotted and tested for statistical significance with MATLAB, R and GraphPad
769 Prism v10. Statistical tests are described in the figure legends. Multiple comparisons with single
770 variables were analyzed with one-way ANOVA with post-hoc Tukey test (comparing the mean of
771 each column with that of every other column). For multiple comparisons with more than one
772 variable, two-way ANOVA with post hoc Tukey or Sidak test was used. The relationships
773 between TRAPed cell counts and freezing levels were analyzed using a partial least-squares
774 analysis implemented in R. Resampling statistics were used to determine the reliability of brain
775 region saliences. The reliability of brain region saliences was determined using bootstrap ratios
776 in which subjects retained their freezing levels but were resampled with replacement 1000
777 times. Original saliences were divided by the bootstrap-derived standard deviations to generate
778 bootstrap ratios (saliences). Salience above 3 was considered reliable. For the correlations
779 shown in Figure 2, all possible pairwise correlations between the TRAP signal in the 29 regions
780 were determined by computing Pearson correlation coefficients. Each complete set of
781 correlations was displayed as color-coded correlation matrices using MATLAB. The Fisher Z-
782 Transformation (to transform the sampling distribution of Pearson's R) was performed in
783 MATLAB. No statistical methods were used to predetermine sample size. Sample sizes were
784 determined based on similar published studies. In all figures, graphs show group means
785 superimposed on individual data points from each animal.

786 Supplemental Information Titles & Legends

787 **Figure S1. Developmental changes in fear memory networks. Related to Figure 1.**
788 Correlation matrices showing the differences in functional connectivity (Fisher Z-transformation)
789 between ages. Fisher correlation coefficients (scale, right; brown and cobalt representing
790 significant differences that are higher in older or younger age groups respectively) and labels
791 within squares correspond to p values of pairwise comparisons of Fisher r-to-z-transformation of

792 the Pearson's correlation coefficient matrices corresponding to respective age groups. *P< 0.05,
793 **P<0.01, ***P<0.001 by one-way ANOVA test.
794
795 **Figure S2. Layer-specific distribution of TRAPed and Fos+ cells in ACA and RSP. Related**
796 **to Figure 3.**
797 (A_1) TRAPed cell distributions across layers in RSP ($F_{layer}(2,33)=45.06$, $P<0.0001$;
798 $F_{age}(2,33)=0.00005$, $P=0.99$; $F_{int}(4,33)=0.96$, $P=0.43$; Infant: N=4; Juvenile: N=5, Adult: N=5).:
799 (A_2) Fos+ cell distribution across layers in RSP: $F_{layer}(2,33)=93.86$, $P<0.0001$; $F_{age}(2,33)=0.0003$,
800 $P=0.99$; $F_{int}(4,33)=0.23$, $P=0.91$; Infant: N=4; Juvenile: N=5, Adult: N=5).
801 (A_3) Reactivated cell distribution across layers in RSP ($F_{layer}(2,33)=8.55$, $P=0.001$;
802 $F_{age}(2,33)=7.97$, $P=0.002$; $F_{int}(4,33)=0.53$, $P=0.71$; Infant: N=4; Juvenile: N=5, Adult: N=5).
803 (B_1) TRAPed cell distributions across layers in ACA ($F_{layer}(2,48)=23.82$, $P<0.0001$;
804 $F_{age}(2,48)=0.0005$, P=99; $F_{int}(4,48)=4.25$, $P=0.005$; Infant: N=4; Juvenile: N=8, Adult: N=7).
805 (B_2) Fos+ cell distribution across layers in ACA ($F_{layer}(2,48)=20.99$, $P<0.0001$;
806 $F_{age}(2,48)=0.0012$, $P=0.99$; $F_{int}(4,48)=5.34$, $P=0.0012$; Infant: N=4; Juvenile: N=8, Adult: N=7).
807 (B_3) Reactivated cell distribution across layers in ACA ($F_{layer}(2,48)=0.51$, $P=0.60$;
808 $F_{age}(2,48)=1.11$, $P=0.33$; $F_{int}(4,48)=0.14$, $P=0.96$; Infant: N=4; Juvenile: N=8, Adult: N=7).
809
810 **Figure S3. Mapping viral targeting in RSP. Related to Figure 4.**
811 (A) Coronal sections showing location of RSP hM3D-mCherry expression in infant-TRAPed
812 mice
813 (B) Coronal sections showing location of RSP hM3D-mCherry expression in juvenile-TRAPed
814 mice
815 (C) Coronal sections showing location of RSP hM3D-mCherry expression in adult-TRAPed mice
816 **Figure S4. RSP Fos levels in hM3D-expressing vs. control mice. Related to Figure 4.**
817 (A_1) Example images RSP showing AAV-mCherry and Fos+ RSP cells infant-TRAPed mice.
818 (A_2). Quantification of Fos+ cell density in RSP for infant-TRAPed mice (Cont: N=4, hM3Dq:
819 N=5, P=0.003, two-tailed t-test).
820 (B_1). Example images RSP showing AAV-mCherry and Fos+ RSP cells infant-TRAPed mice.
821 in juvenile-TRAPed mice (Cont: N=6, hM3Dq: N=6, P=0.0001, two-tailed t-test).
822 (B_2). Quantification of Fos+ cell density in RSP for juvenile-TRAPed mice.
823 (C_1). Example images RSP showing AAV-mCherry and Fos+ RSP cells adult-TRAPed mice.
824 (C_2). Quantification of Fos+ cell density in RSP for adult -TRAPed mice (Cont: N=6, hM3Dq:
825 N=6, P<0.0001, two-tailed t-test).

826 Scale bars, 125 μm. Graphs show mean ± SEM.
827
828 **Figure S5. Mapping viral targeting in RSP. Related to Figure 5.**
829 (A) Coronal sections showing location of RSP hM3D-mCherry expression in infant-TRAPed
830 mice.
831 (B) Example images RSP showing AAV-mCherry and Fos+ RSP cells infant-TRAPed mice.
832 Scale bars, 125μm.
833 (C) Quantification of Fos+ cell density in RSP for infant-TRAPed mice (Cont: N=6, hM3Dq: N=6,
834 P<0.0001, two-tailed t-test). Graphs show mean ± SEM.
835
836 **Figure S6. RSP DREADD validation and controls for Figure 5.**
837 (A) Representative coronal section showing AAV-hM3Dq injection sites in LSX and ACA.
838 (B) Percent freezing levels in contexts A and B during the 33d retrieval test in LSX- and ACA-
839 targeted mice (LSX: P=0.54, N=3, ACA: P=0.56, N=3, paired t-test). Graphs show mean ± SEM.

840 # References

841 1. Bauer, P. J. & Larkina, M. Childhood amnesia in the making: Different distributions of
842 autobiographical memories in children and adults. *J. Exp. Psychol. Gen.* **143**, 597–611
843 (2014).
844 2. Bauer, P. J., Tasdemir-Ozdes, A. & Larkina, M. Adults' reports of their earliest memories:
845 Consistency in events, ages, and narrative characteristics over time. *Conscious. Cogn.* **27**,
846 76–88 (2014).
847 3. Campbell, B. A. & Campbell, E. H. Retention and extinction of learned fear in infant and
848 adult rats. *J. Comp. Physiol. Psychol.* **55**, 1–8 (1962).
849 4. Lloyd, M. E. & Newcombe, N. S. Implicit memory in childhood: Reassessing developmental
850 invariance. in *The development of memory in infancy and childhood, 2nd ed.* 93–113
851 (Psychology Press, 2009).
852 5. Ramsaran, A. I., Schlichting, M. L. & Frankland, P. W. The ontogeny of memory persistence
853 and specificity. *Dev. Cogn. Neurosci.* (2018) doi:10.1016/j.dcn.2018.09.002.
854 6. Campbell, B. A. & Spear, N. E. *ONTOGENY OF MEMORY 1*. *Psychological Review* vol. 79
855 215–236 (1972).
856 7. Callaghan, B. *et al.* Using a Developmental Ecology Framework to Align Fear Neurobiology
857 Across Species. *Annu. Rev. Clin. Psychol.* (2019) doi:10.1146/annurev-clinpsy-050718-
858 095727.

859 8. Akers, K. G., Arruda-Carvalho, M., Josselyn, S. A. & Frankland, P. W. Ontogeny of
860 contextual fear memory formation, specificity, and persistence in mice. *Learn. Mem.* **19**,
861 598–604 (2012).
862 9. Akers, K. G. *et al.* Hippocampal Neurogenesis Regulates Forgetting During Adulthood and
863 Infancy. *Science* **598**, 598–603 (2014).
864 10. Guskjolen, A., Josselyn, S. A. & Frankland, P. W. Age-dependent changes in spatial
865 memory retention and flexibility in mice. *Ontog. Learn. Mem.* **143**, 59–66 (2017).
866 11. Guskjolen, A. *et al.* Recovery of "Lost" Infant Memories in Mice. *Curr. Biol.* 1–8 (2018)
867 doi:10.1016/j.cub.2018.05.059.
868 12. Li, S., Kim, J. H. & Richardson, R. Updating memories: Changing the involvement of the
869 prelimbic cortex in the expression of an infant fear memory. *Neuroscience* **222**, 316–325
870 (2012).
871 13. Travaglia, A., Bisaz, R., Sweet, E. S., Blitzer, R. D. & Alberini, C. M. Infantile amnesia
872 reflects a developmental critical period for hippocampal learning. *Nat. Neurosci.* **19**, 1225–
873 1233 (2016).
874 14. Alberini, C. M. & Travaglia, A. Infantile Amnesia: A Critical Period of Learning to Learn and
875 Remember. *J. Neurosci.* **37**, 5783–5795 (2017).
876 15. Kim, J. H., Li, S., Hamlin, A. S., McNally, G. P. & Richardson, R. Phosphorylation of
877 mitogen-activated protein kinase in the medial prefrontal cortex and the amygdala following
878 memory retrieval or forgetting in developing rats. *Neurobiol. Learn. Mem.* **97**, 59–68 (2012).
879 16. Spear, N. & Parsons, P. Analysis of a reactivation treatment: Ontogenetic determinants of
880 alleviated forgetting. in *Processes of Animal Memory* vol. 1 135–165 (Lawrence Erlbaum
881 Associates, 1976).
882 17. Campbell, B. A. & Jaynes, J. Reinstatement. *Psychol. Rev.* **73**, 478–480 (1966).
883 18. Callaghan, B. L. & Richardson, R. Maternal Separation Results in Early Emergence of
884 Adult-Like Fear and Extinction Learning in Infant Rats. *Behav. Neurosci.* (2011)
885 doi:10.1037/a0022008.
886 19. Bath, K. G., Manzano-Nieves, G. & Goodwill, H. Early life stress accelerates behavioral and
887 neural maturation of the hippocampus in male mice. *Horm. Behav.* (2016)
888 doi:10.1016/j.yhbeh.2016.04.010.
889 20. Callaghan, B. L. & Tottenham, N. The Stress Acceleration Hypothesis: Effects of early-life
890 adversity on emotion circuits and behavior. *Curr. Opin. Behav. Sci.* **7**, 76–81 (2016).
891 21. Frankland, P. W. & Bontempi, B. The organization of recent and remote memories. *Nat.*
892 *Rev. Neurosci.* **6**, 119–30 (2005).

22. Frankland, P. W. & Bontempi, B. Fast track to the medial prefrontal cortex. *Pnas* **103**, 509–510 (2006).
23. Tonegawa, S., Morrissey, M. D. & Kitamura, T. The role of engram cells in the systems consolidation of memory. *Nat. Rev. Neurosci.* **19**, 485–498 (2018).
24. Klune, C. B., Jin, B. & DeNardo, L. A. Linking mPFC circuit maturation to the developmental regulation of emotional memory and cognitive flexibility. *eLife* **10**, 1–33 (2021).
25. Sugar, J. & Witter, M. P. Postnatal development of retrosplenial projections to the parahippocampal region of the rat. *eLife* **5**, e13925 (2016).
26. Haugland, K. G., Sugar, J. & Witter, M. P. Development and topographical organization of projections from the hippocampus and parahippocampus to the retrosplenial cortex. *Eur. J. Neurosci.* **50**, 1799–1819 (2019).
27. DeNardo, L. & Luo, L. Genetic strategies to access activated neurons. *Curr Opin Neurobiol* **45**, 121–129 (2017).
28. Allen, W. E. *et al.* Thirst-associated preoptic neurons encode an aversive motivational drive. *Science* **357**, 1149–1155 (2017).
29. DeNardo, L. A. *et al.* Temporal evolution of cortical ensembles promoting remote memory retrieval. *Nat. Neurosci.* **22**, 460–469 (2019).
30. Michael W. Gongwer *et al.* Brain-wide projections and differential encoding of prefrontal neuronal classes underlying learned and innate threat avoidance. *J. Neurosci.* JN-RM-0697-23 (2023) doi:10.1523/JNEUROSCI.0697-23.2023.
31. Madisen, L. *et al.* A robust and high-throughput Cre reporting and characterization system for the whole mouse brain. *Nat. Neurosci.* **13**, 133–140 (2010).
32. Chi, J. *et al.* Three-Dimensional Adipose Tissue Imaging Reveals Regional Variation in Beige Fat Biogenesis and PRDM16-Dependent Sympathetic Neurite Density. *Cell Metab.* (2018) doi:10.1016/j.cmet.2017.12.011.
33. Do Monte, F., Quirk, G., Li, B. & Penzo, M. Retrieving fear memories, as time goes by…. *Mol. Psychiatry* **21**, 1027–1036 (2016).
34. Kwapis, J. L., Jarome, T. J., Lee, J. L. & Helmstetter, F. J. The retrosplenial cortex is involved in the formation of memory for context and trace fear conditioning. *Neurobiol. Learn. Mem.* **123**, 110–116 (2015).
35. Corcoran, K. A., Frick, B. J., Radulovic, J. & Kay, L. M. Analysis of coherent activity between retrosplenial cortex, hippocampus, thalamus, and anterior cingulate cortex during retrieval of recent and remote context fear memory. *Neurobiol. Learn. Mem.* **127**, 93–101 (2016).
36. Marchand, A., Faugère, A., Coutureau, E. & Wolff, M. A role for anterior thalamic nuclei in

927 contextual fear memory. *Brain Struct. Funct.* **219**, 1575–1586 (2014).
928 37. Vetere, G. *et al.* An inhibitory hippocampal–thalamic pathway modulates remote memory
929 retrieval. *Nat. Neurosci.* **24**, 685–693 (2021).
930 38. Wheeler, A. L. *et al.* Identification of a Functional Connectome for Long-Term Fear Memory
931 in Mice. *PLoS Comput. Biol.* **9**, e1002853 (2013).
932 39. Vetere, G. *et al.* Chemogenetic Interrogation of a Brain-wide Fear Memory Network in Mice.
933 *Neuron* **94**, 363–374 (2017).
934 40. De Sousa, A. F. *et al.* Optogenetic reactivation of memory ensembles in the retrosplenial
935 cortex induces systems consolidation. *Proc. Natl. Acad. Sci. U. S. A.* **116**, 8576–8581
936 (2019).
937 41. Trask, S., Ferrara, N. C., Jasnow, A. M. & Kwapis, J. L. Contributions of the rodent
938 cingulate-retrosplenial cortical axis to associative learning and memory: A proposed circuit
939 for persistent memory maintenance. *Neurosci. Biobehav. Rev.* **130**, 178–184 (2021).
940 42. Keene, C. S. & Bucci, D. J. Contributions of the retrosplenial and posterior parietal cortices
941 to cue-specific and contextual fear conditioning. *Behav. Neurosci.* **122**, 89–97 (2008).
942 43. Frankland, P. W., Josselyn, S. A. & Köhler, S. The neurobiological foundation of memory
943 retrieval. *Nat. Neurosci.* **22**, 1576–1585 (2019).
944 44. Tonegawa, S., Liu, X., Ramirez, S. & Redondo, R. Memory Engram Cells Have Come of
945 Age. *Neuron* **87**, 918–931 (2015).
946 45. Josselyn, S. A. & Tonegawa, S. Memory engrams: Recalling the past and imagining the
947 future. *Science* **367**, (2020).
948 46. Kitamura, T. *et al.* Engrams and circuits crucial for systems consolidation of a memory.
949 *Science* **356**, 73–78 (2017).
950 47. Todd, T. P., Mehlman, M. L., Keene, C. S., DeAngeli, N. E. & Bucci, D. J. Retrosplenial
951 cortex is required for the retrieval of remote memory for auditory cues. *Learn. Mem. Cold*
952 *Spring Harb. N* **23**, 278–88 (2016).
953 48. Harris, K. D. & Shepherd, G. M. G. The neocortical circuit: Themes and variations. *Nat.*
954 *Neurosci.* **18**, 170–181 (2015).
955 49. Armbruster, B. N., Li, X., Pausch, M. H., Herlitze, S. & Roth, B. L. Evolving the lock to fit the
956 key to create a family of G protein-coupled receptors potently activated by an inert ligand.
957 *Proc. Natl. Acad. Sci.* **104**, 5163–5168 (2007).
958 50. Sugar, J., Witter, M., van Strien, N. & Cappaert, N. The Retrosplenial Cortex: Intrinsic
959 Connectivity and Connections with the (Para)Hippocampal Region in the Rat. An Interactive
960 Connectome. *Front. Neuroinformatics* **5**, (2011).

961 51. van Groen, T. & Michael Wyss, J. Connections of the retrosplenial granular a cortex in the
962 rat. *J. Comp. Neurol.* **300**, 593–606 (1990).
963 52. van Groen, T. & Wyss, J. M. Connections of the retrosplenial dysgranular cortex in the rat.
964 *J. Comp. Neurol.* **315**, 200–216 (1992).
965 53. Vann, S. D., Aggleton, J. P. & Maguire, E. A. What does the retrosplenial cortex do? *Nat.*
966 *Rev. Neurosci.* **10**, 792–802 (2009).
967 54. Li, S., Callaghan, B. L. & Richardson, R. Infantile amnesia: Forgotten but not gone. *Learn.*
968 *Mem.* **21**, 135–139 (2014).
969 55. Axel Guskjolen *et al.* Neurogenesis-mediated circuit remodeling reduces engram
970 reinstatement and promotes forgetting. *bioRxiv* 2023.10.10.561722 (2023)
971 doi:10.1101/2023.10.10.561722.
972 56. Miller, A. M. P., Vedder, L. C., Law, L. M. & Smith, D. M. Cues, context, and long-term
973 memory: the role of the retrosplenial cortex in spatial cognition. *Front. Hum. Neurosci.* **8**,
974 (2014).
975 57. Maviel, T. Sites of Neocortical Reorganization Critical for Remote Spatial Memory. *Science*
976 **305**, 96–99 (2004).
977 58. Thomas Wolbers & Christian Büchel. Dissociable Retrosplenial and Hippocampal
978 Contributions to Successful Formation of Survey Representations. *J. Neurosci.* **25**, 3333
979 (2005).
980 59. Staresina, B. P., Alink, A., Kriegeskorte, N. & Henson, R. N. Awake reactivation predicts
981 memory in humans. *Proc. Natl. Acad. Sci.* **110**, 21159–21164 (2013).
982 60. Opalka, A. N. & Wang, D. V. Hippocampal efferents to retrosplenial cortex and lateral
983 septum are required for memory acquisition. *Learn. Mem.* **27**, 310–318 (2020).
984 61. Katche, C. *et al.* On the role of retrosplenial cortex in long-lasting memory storage.
985 *Hippocampus* **23**, 295–302 (2013).
986 62. Keene, C. S. & Bucci, D. J. Neurotoxic lesions of retrosplenial cortex disrupt signaled and
987 unsignaled contextual fear conditioning. *Behav. Neurosci.* **122**, 1070–1077 (2008).
988 63. Robinson, S., Keene, C. S., Iaccarino, H. F., Duan, D. & Bucci, D. J. Involvement of
989 retrosplenial cortex in forming associations between multiple sensory stimuli. *Behav.*
990 *Neurosci.* **125**, 578–587 (2011).
991 64. Freeman, J. H. & Gabriel, M. Changes of Cingulothalamic Topographic Excitation Patterns
992 and Avoidance Response Incubation over Time Following Initial Discriminative Conditioning
993 in Rabbits. *Neurobiol. Learn. Mem.* **72**, 259–272 (1999).
994 65. Bussey, T. J., Muir, J. L., Everitt, B. J. & Robbins, T. W. Dissociable effects of anterior and

995 posterior cingulate cortex lesions on the acquisition of a conditional visual discrimination:
996 Facilitation of early learning vs. impairment of late learning. *Behav. Brain Res.* **82**, 45–56
997 (1996).
998 66. Corcoran, K. A. *et al.* NMDA Receptors in Retrosplenial Cortex Are Necessary for Retrieval
999 of Recent and Remote Context Fear Memory. *J. Neurosci.* **31**, 11655–11659 (2011).
1000 67. VALENSTEIN, E. *et al.* RETROSPLENIAL AMNESIA. *Brain* **110**, 1631–1646 (1987).
1001 68. Gainotti, G., Almonti, S., Di Betta, A. M. & Silveri, M. C. Retrograde amnesia in a patient
1002 with retrosplenial tumour. *Neurocase* **4**, 519–526 (1998).
1003 69. Cowansage, K. K. *et al.* Direct Reactivation of a Coherent Neocortical Memory of Context.
1004 *Neuron* **84**, 432–441 (2014).
1005 70. Aggleton, J. P. EPS Mid-Career Award 2006: Understanding anterograde amnesia:
1006 Disconnections and hidden lesions. *Q. J. Exp. Psychol.* **61**, 1441–1471 (2008).
1007 71. Insausti, R., Amaral, D. G. & Cowan, W. M. The entorhinal cortex of the monkey: II. Cortical
1008 afferents. *J. Comp. Neurol.* **264**, 356–395 (1987).
1009 72. van Groen, T. & Michael Wyss, J. Connections of the retrosplenial granular a cortex in the
1010 rat. *J. Comp. Neurol.* **300**, 593–606 (1990).
1011 73. van Groen, T. & Wyss, J. M. Connections of the retrosplenial dysgranular cortex in the rat.
1012 *J. Comp. Neurol.* **315**, 200–216 (1992).
1013 74. Van Groen, T. & Wyss, J. M. Connections of the retrosplenial granular b cortex in the rat. *J.*
1014 *Comp. Neurol.* **463**, 249–263 (2003).
1015 75. WA Suzuki & DG Amaral. Topographic organization of the reciprocal connections between
1016 the monkey entorhinal cortex and the perirhinal and parahippocampal cortices. *J. Neurosci.*
1017 **14**, 1856 (1994).
1018 76. Burwell, R. D. & Amaral, D. G. Cortical afferents of the perirhinal, postrhinal, and entorhinal
1019 cortices of the rat. *J. Comp. Neurol.* **398**, 179–205 (1998).
1020 77. Morris, R., Petrides, M. & Pandya, D. N. Architecture and connections of retrosplenial area
1021 30 in the rhesus monkey (macaca mulatta). *Eur. J. Neurosci.* **11**, 2506–2518 (1999).
1022 78. Lavenex, P., Suzuki, W. A. & Amaral, D. G. Perirhinal and parahippocampal cortices of the
1023 macaque monkey: Projections to the neocortex. *J. Comp. Neurol.* **447**, 394–420 (2002).
1024 79. Kobayashi, Y. & Amaral, D. G. Macaque monkey retrosplenial cortex: II. Cortical afferents.
1025 *J. Comp. Neurol.* **466**, 48–79 (2003).
1026 80. Choi, H. *et al.* Maturation of metabolic connectivity of the adolescent rat brain. *eLife* **4**,
1027 e11571 (2015).
1028 81. Yasuno, F. *et al.* Resting-state synchrony between the retrosplenial cortex and anterior

1029 medial cortical structures relates to memory complaints in subjective cognitive impairment.
1030 *Neurobiol. Aging* **36**, 2145–2152 (2015).
1031 82. Düzel, E., Schütze, H., Yonelinas, A. P. & Heinze, H. Functional phenotyping of successful
1032 aging in long-term memory: Preserved performance in the absence of neural compensation.
1033 *Hippocampus* **21**, 803–814 (2011).
1034 83. Callaghan, B. L., Li, S. & Richardson, R. The elusive engram: what can infantile amnesia tell
1035 us about memory? *Trends Neurosci.* **37**, 47–53 (2014).
1036 84. Arruda-Carvalho, M., Wu, W.-C., Cummings, K. A. & Clem, R. L. Optogenetic Examination
1037 of Prefrontal-Amygdala Synaptic Development. *J. Neurosci.* **37**, 2976–2985 (2017).
1038 85. Mathis, A. *et al.* DeepLabCut: markerless pose estimation of user-defined body parts with
1039 deep learning. *Nat. Neurosci.* **21**, (2018).
1040 86. Gabriel, C. J. *et al.* Behavior DEPOT is a simple, flexible tool for automated behavioral
1041 detection based on marker less pose tracking. *eLife* **11**, 1–33 (2022).
1042 87. Friedmann, D. *et al.* Mapping mesoscale axonal projections in the mouse brain using a 3D
1043 convolutional network. *Proc. Natl. Acad. Sci.* (2020) doi:10.1073/pnas.1918465117.
1044 88. Wang, Q. *et al.* The Allen Mouse Brain Common Coordinate Framework: A 3D Reference
1045 Atlas. *Cell* **181**, 936-953.e20 (2020).
1046 89. Carey, H. *et al.* DeepSlice: rapid fully automatic registration of mouse brain imaging to a
1047 volumetric atlas. *Nat. Commun.* **14**, 5884 (2023).
1048 90. Schindelin, J. *et al.* Fiji: an open-source platform for biological-image analysis. *Nat. Methods*
1049 **9**, 676–682 (2012).
1050 91. Chiaruttini, N. *et al.* An Open-Source Whole Slide Image Registration Workflow at Cellular
1051 Precision Using Fiji, QuPath and Elastix. *Front. Comput. Sci.* **3**, (2022).
1052
1053

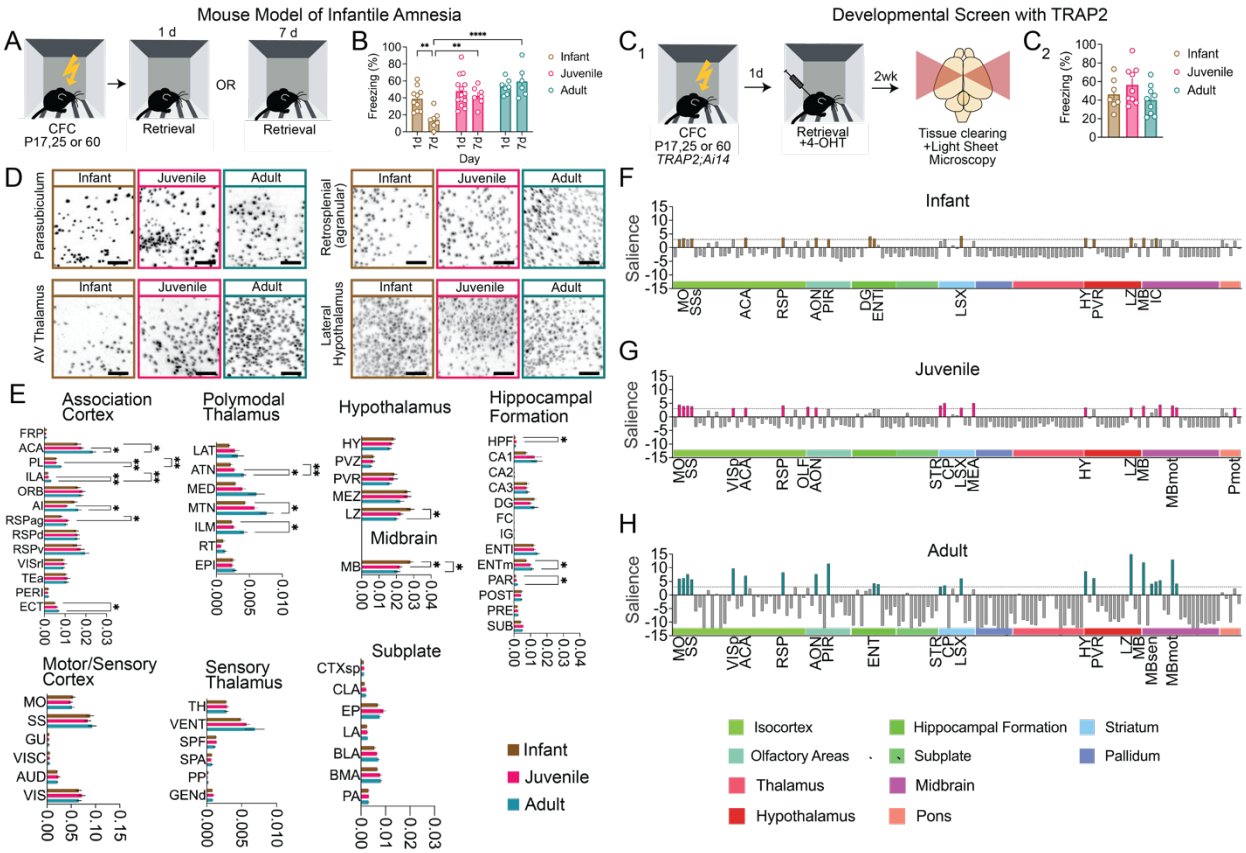

Figure 1. A developmental screen to identify neural signatures of infantile amnesia.
(A) Infant, juvenile, and adult mice underwent contextual fear conditioning and then memory testing 1 or 7 days later.
(B) Percent time freezing in infant, juvenile and adult wildtype mice during memory retrieval tests occurring 1 or 7 days after CFC ($F_{age}(2,45)=15.89$, $P<0.0001$, $F_{day}(1,45)=3.56$, $P=0.07$, $F_{int}(2,45)=4.21$, $P=0.02$, Infant: N=7 1d, N=10 7d; Juvenile: N=14 1d, N=8 7d; Adult: N=7 1d, N=6 7d, two-way ANOVA with Tukey post-hoc test).
(C_1) Experimental design for developmental screen.
(C_2) Freezing behavior in TRAP mice used in screen ($F(2,22)=1.87$, $P=0.18$, One way ANOVA; N=7 infant, N=9 juvenile, N=9 adult).
(D) Representative 100-µm thick optical z-stacks showing TRAPed cells from 1-day retrieval.
(E) TRAPed cell counts by age (Sensory cortex: $F_{region}(2.03,44.7)=267.30$, $P<0.0001$; $F_{age}(2,22)=0.02$, $P=0.97$; $F_{int}(10,110)=0.65$, $P=0.77$; Association cortex: $F_{region}(3.45,75.93)=132.7$, $P<0.0001$; $F_{age}(2,22)=3.82$, $P=0.38$; $F_{int}(24,264)=2.14$, $P=0.002$; Sensory Thalamus: $F_{region}(1.18,26.04)=80.39$, $P<0.0001$; $F_{age}(2,22)=0.69$, $P=0.51$; $F_{int}(10,110)=1.05$, $P=0.41$; Polymodal thalamus: $F_{region}(2.22,48.84)=28.77$, $P<0.0001$; $F_{age}(2,22)=7.60$, $P=0.003$; $F_{int}(12,132)=1.59$, $P=0.10$; Hypothalamus/Midbrain: $F_{region}(3.38,74.38)=141.0$, $P<0.0001$; $F_{age}(2,22)=3.10$, $P=0.07$; $F_{int}(10,110)=2.61$, $P=0.007$; Subplate: $F_{region}(2.96,65.07)=149.7$, $P<0.0001$; $F_{age}(2,22)=1.93$, $P=0.17$; $F_{int}(12,132)=1.42$, $P=0.17$; Hippocampal Formation: $F_{region}(1.94,42.58)=43.78$, $P<0.0001$; $F_{age}(2,22)=2.16$, $P=0.14$; $F_{int}(24,264)=0.82$, $P=0.72$. Infant N=7, Juvenile N=9, Adult N=9; Two-way repeated measure ANOVAs with Tukey post-hoc correction test).
(F-H) Task PLS analysis of TRAPed cell densities in (F) infants, (G) juveniles and (H) adults. Dashed lines indicate threshold of 3. Color labels on x-axis correspond to major brain subdivisions according to the Allen Brain Atlas.
See Tables S1 and S2 for abbreviations and statistics. Graphs show mean ± SEM. *P< 0.05, **P<0.01, ***P<0.001. Scale bars, 100 µm.

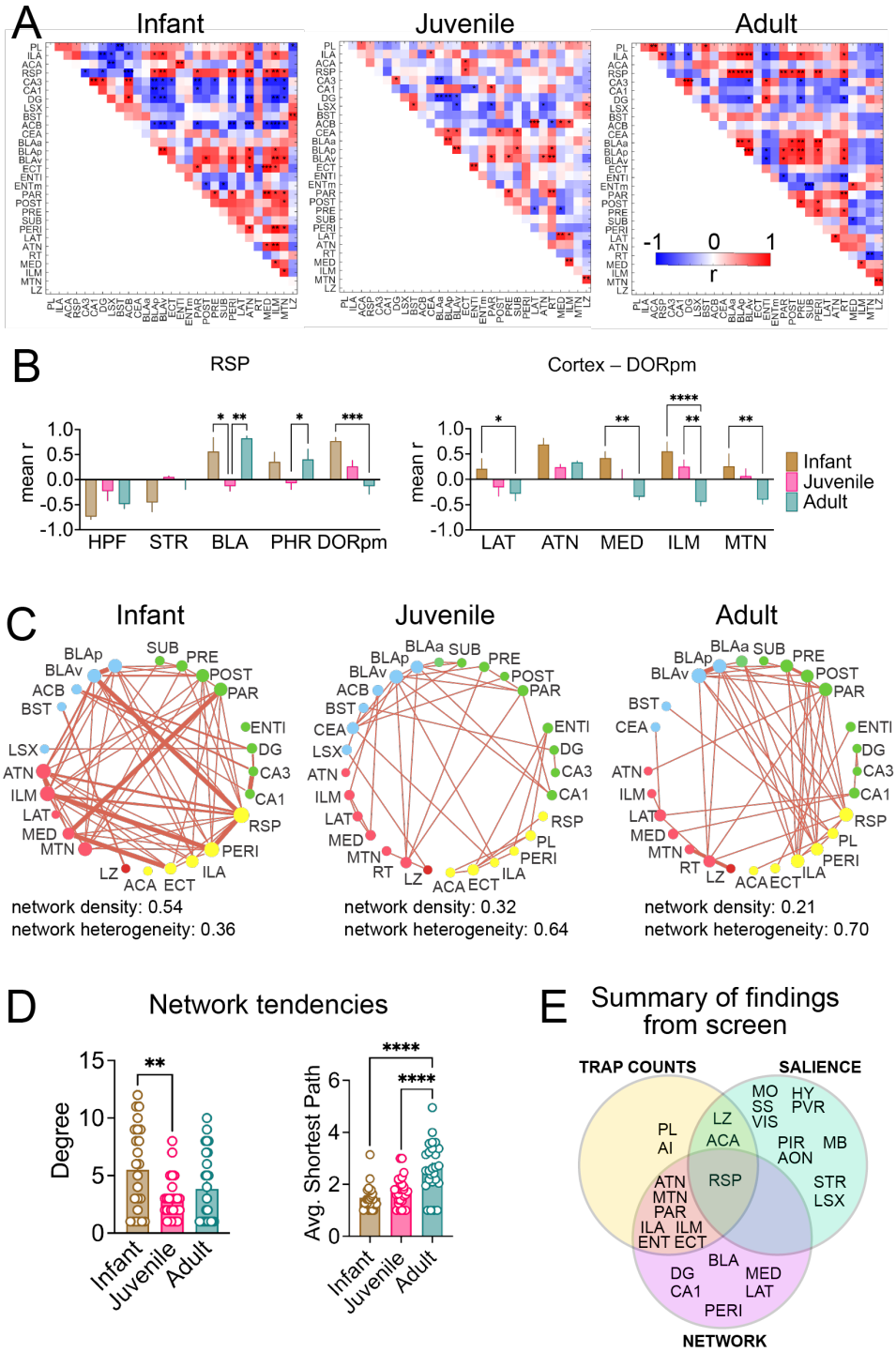

Figure 2. Developmental changes in fear memory networks.
(A) Pearson correlation matrices showing interregional correlations based on numbers of TRAPed cells at 1-day memory retrieval across ages. Colors reflect Pearson correlation coefficients (scale, right) and labels within squares correspond to p values from pairwise comparisons.
(B) Mean pearson r values for left: RSP ($F_{region}(4,48) = 12.47$, $P<0.0001$; $F_{age}(2,48) = 1.04$, $P=0.37$; $F_{interaction}(8,48) = 5.60$, $P<0.0001$; HPF: N=3; STR: N=4; BLA: N=3; PHR: N=6; TH: N=5 brain regions) and right: between dorsal cortex (PL, ILA, ACA, RSP) and dorsal polymodal thalamic nuclei (DORpm, $F_{region}(4, 45) = 5.82$, $P=0.0007$; $F_{age}(2, 45) = 26.48$, $P<0.0001$; $F_{interaction}(8, 45) = 1.36$, $P=0.24$; N=4 cortical brain regions). Two-way ANOVAs with Tukey post-

hoc correction test.
(C) Network graphs generated for Pearson's correlations $p<0.1$ Regions are grouped and colored according to major brain subdivision as defined by the Allen Brain Atlas. The node size is proportional to the number of connections (degree) and the weights of the lines are proportional to the correlation strength.
(D) Average degree (left, $F(2,75)=5.21$, $P=0.008$, One-way ANOVA) and shortest path length (right, $F(2,75)=18.34$, $P<0.0001$, One-way ANOVA) for each network node for each age (Infant: N=24; Juvenile: N=28; Adult: N=26 nodes).
(E) Summary of convergent findings from analyses presented in Figures 1 and 2.
*$P< 0.05$, **$P<0.01$, ***$P<0.001$, ****$P<0.0001$. Graphs show mean $\pm$ SEM. See also Figure S1 for additional network analyses.

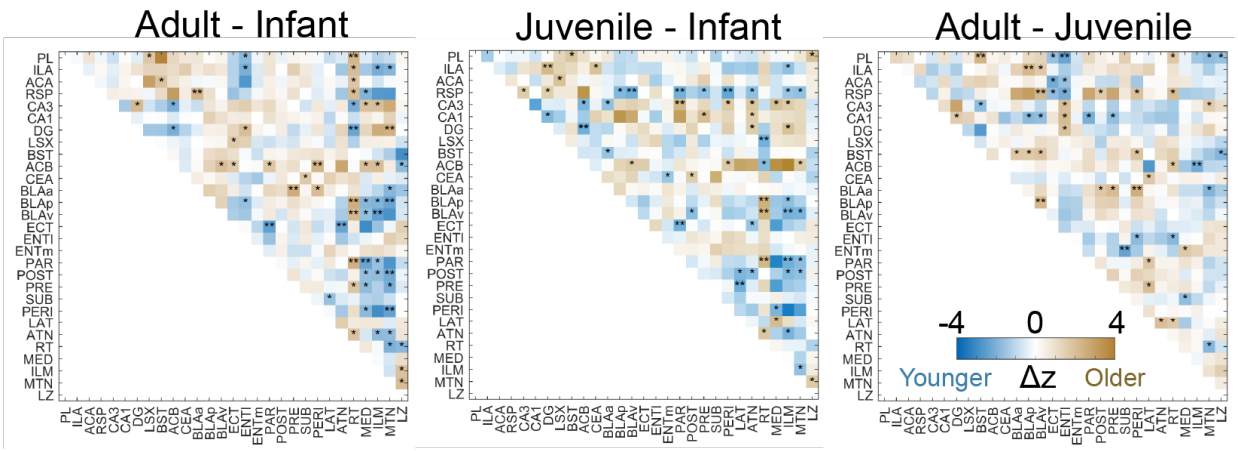

Figure S1. Developmental changes in fear memory networks. Related to Figure 1. Correlation matrices showing the differences in functional connectivity (Fisher Z-transformation) between ages. Fisher correlation coefficients (scale, right; brown and cobalt representing significant differences that are higher in older or younger age groups respectively) and labels within squares correspond to p values of pairwise comparisons of Fisher r-to-z-transformation of the Pearson's correlation coefficient matrices corresponding to respective age groups. *P< 0.05, **P<0.01, ***P<0.001 by one-way ANOVA test.

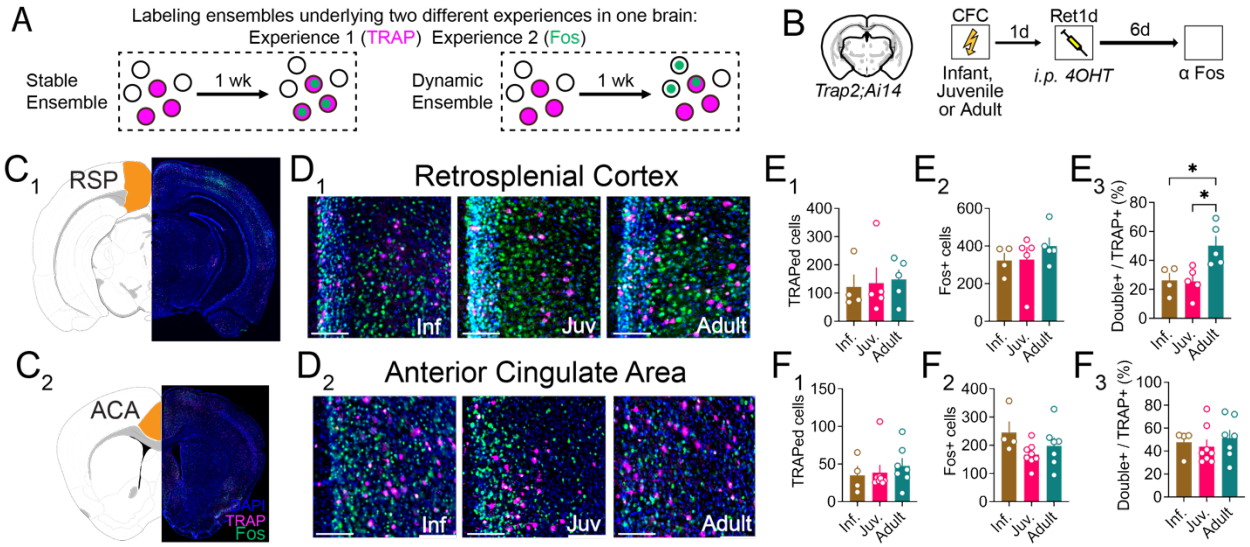

Figure 3. Selectively increased reactivation of memory-encoding ensembles in RSP in adults.

(A) Illustration of stable vs. dynamic ensembles in a TRAP/Fos overlay assay.

(B) Experiment design for activity-dependent tagging of ensembles between 1- and 7-day retrieval.

(C) Illustration of analysis sites for RSP and ACA.

(D) Representative examples of TRAPed (magenta) and Fos+ cells (green) in the anterior cingulate (top) and retrosplenial cortices (anterior, middle; posterior, bottom).

(E_1) TRAPed cells per ROI for ACA ($F(2,16)=0.34$, $P=0.72$, one-way ANOVA with Tukey post-hoc correction; Infant: N=4, Juvenile: N=8, Adult: N=7).

(E_2) Fos+ cells per ROI for ACA each region and age group ($F(2,16)=2.11$, $P=0.15$, one-way ANOVA with Tukey post-hoc correction; Infant: N=4, Juvenile: N=8, Adult: N=7).

(E_3) Double-labeled neurons per ROI for ACA ($F(2,16)=0.39$, $P=0.68$, one-way ANOVA with Tukey post-hoc correction; Infant: N=4, Juvenile: N=8, Adult: N=7).

(F_1) TRAPed cells per ROI for RSP ($F(2,11)=0.09$, $P=0.92$, one-way ANOVA with Tukey post-hoc correction; Infant: N=4, Juvenile: N=5, Adult: N=5).

(F_2) Fos+ cells per ROI for RSP each region and age group ($F(2,11)=0.70$, $P=0.52$, one-way ANOVA with Tukey post-hoc correction; Infant: N=4, Juvenile: N=5, Adult: N=5).

(F_3) Double-labeled neurons per ROI for RSP ($F(2,11)=7.1$, $P=0.01$, one-way ANOVA with Tukey post-hoc correction; Infant: N=4, Juvenile: N=5, Adult: N=5).

Graphs show mean ± SEM. *P <0.05. See also Figure S2 for layer analysis.

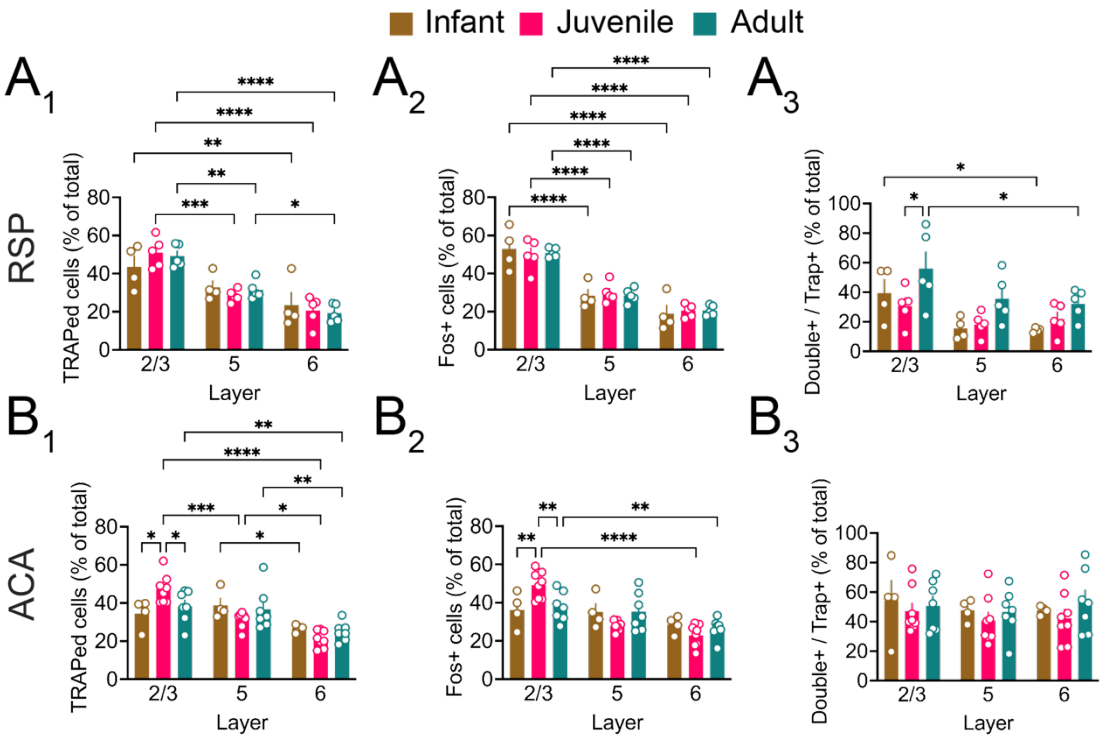

Figure S2. Layer-specific distribution of TRAPed and Fos+ cells in ACA and RSP. Related to Figure 3.

(A_1) TRAPed cell distributions across layers in RSP ($F_{layer}(2,33)=45.06$, $P<0.0001$; $F_{age}(2,33)=0.00005$, $P=0.99$; $F_{int}(4,33)=0.96$, $P=0.43$; Infant: N=4; Juvenile: N=5, Adult: N=5).:
(A_2) Fos+ cell distribution across layers in RSP: $F_{layer}(2,33)=93.86$, $P<0.0001$; $F_{age}(2,33)=0.0003$, $P=0.99$; $F_{int}(4,33)=0.23$, $P=0.91$; Infant: N=4; Juvenile: N=5, Adult: N=5).
(A_3) Reactivated cell distribution across layers in RSP ($F_{layer}(2,33)=8.55$, $P=0.001$; $F_{age}(2,33)=7.97$, $P=0.002$; $F_{int}(4,33)=0.53$, $P=0.71$; Infant: N=4; Juvenile: N=5, Adult: N=5).
(B_1) TRAPed cell distributions across layers in ACA ($F_{layer}(2,48)=23.82$, $P<0.0001$; $F_{age}(2,48)=0.0005$, $P=99$; $F_{int}(4,48)=4.25$, $P=0.005$; Infant: N=4; Juvenile: N=8, Adult: N=7).
(B_2) Fos+ cell distribution across layers in ACA ($F_{layer}(2,48)=20.99$, $P<0.0001$; $F_{age}(2,48)=0.0012$, $P=0.99$; $F_{int}(4,48)=5.34$, $P=0.0012$; Infant: N=4; Juvenile: N=8, Adult: N=7).
(B_3) Reactivated cell distribution across layers in ACA ($F_{layer}(2,48)=0.51$, $P=0.60$; $F_{age}(2,48)=1.11$, $P=0.33$; $F_{int}(4,48)=0.14$, $P=0.96$; Infant: N=4; Juvenile: N=8, Adult: N=7).

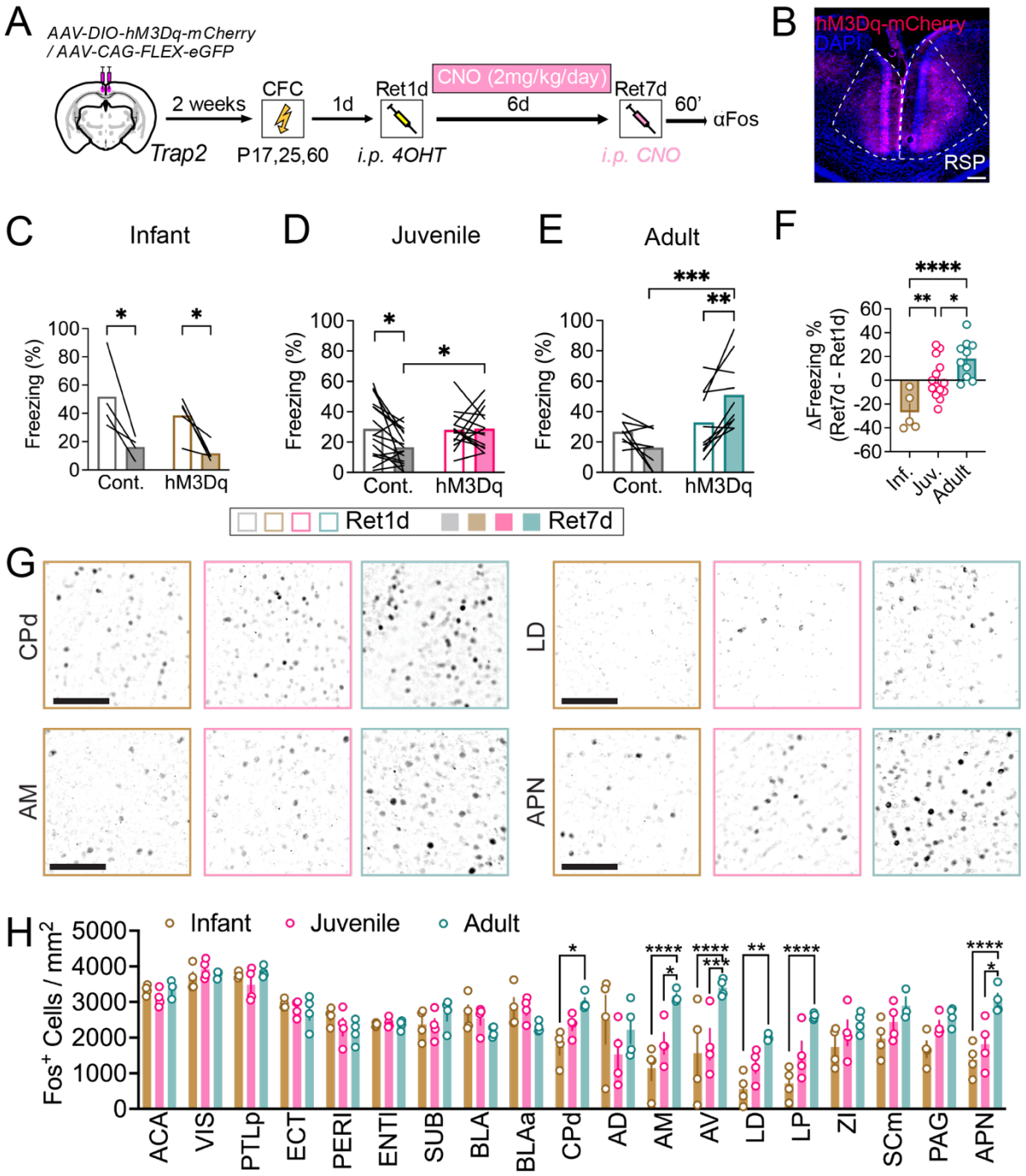

Figure 4. Chemogenetic reactivation of TRAPed RSC neurons increased freezing during short-term memory retrieval in an age-dependent manner.

(A) Experimental design.

(B) Representative coronal section showing AAV injection site in RSP. Scale bar, 125 μm.

(C) Percent freezing levels at 1- and 7-day retrieval in control (grey) and hM3Dq (brown) groups for infants ($F_{virus}(1,7)=1.29$, $P=0.29$, $F_{day}=(1,7)=24.18$, $P=0.002$; $F_{int}(1,7)=0.47$, $P=0.51$, Cont: N=4, hM3Dq: N=5, two-way ANOVA with Holm-Sidak post hoc test).

(D) Percent freezing levels at 1- and 7-day retrieval in control (grey) and hM3Dq (magenta) groups for juveniles ($F_{virus}(1,28)=1.81$, $P=0.19$, $F_{day}=(1,7)=3.33$, $P=0.07$; $F_{int}(1,7)=4.34$, $P=0.04$, Cont: N=16, hM3Dq: N=14, two-way ANOVA with Holm-Sidak post hoc test).

(E) Percent freezing levels at 1- and 7-day retrieval in control (grey) and hM3Dq (teal) groups for adults ($F_{virus}(1,28)=1.81$, $P=0.19$, $F_{day}=(1,7)=3.33$, $P=0.07$; $F_{int}(1,7)=4.34$, $P=0.04$, Cont: N=8, hM3Dq: N=10, two-way ANOVA with Holm-Sidak post hoc test).
(F) Differences in freezing levels between 7-day and 1-day retrieval sessions for hM3Dq mice in each age group ($F(2,26)=12.92$, $P=0.001$, Infant: N=5, Juvenile: N=14, Adult: N=10, one-way ANOVA with Tukey post hoc test).
(G) Representative images showing Fos immunoreactive cells in dorsal caudate putamen (CPd), anteromedial thalamus (AM), laterodorsal thalamus (LD), and anterior pretectal nucleus (APN). Scale bars, 100 µm.
(H) Quantification of Fos+ cells per ROI in 19 brain regions ($F_{region}(18,160)=30.03$, $P<0.05$; $F_{age}(2,9)=3.69$, $P>0.05$; $F_{int}(36,160)=5.78$, $P<0.05$, Mixed Effects Model; Infant: N=4; Juvenile: N=4; Adult: N=3-4).
Graphs show mean $\pm$ SEM. * $P<0.05$, ** $P<0.01$, *** $P<0.001$, **** $P<0.0001$. See also Figure S3 and S4.

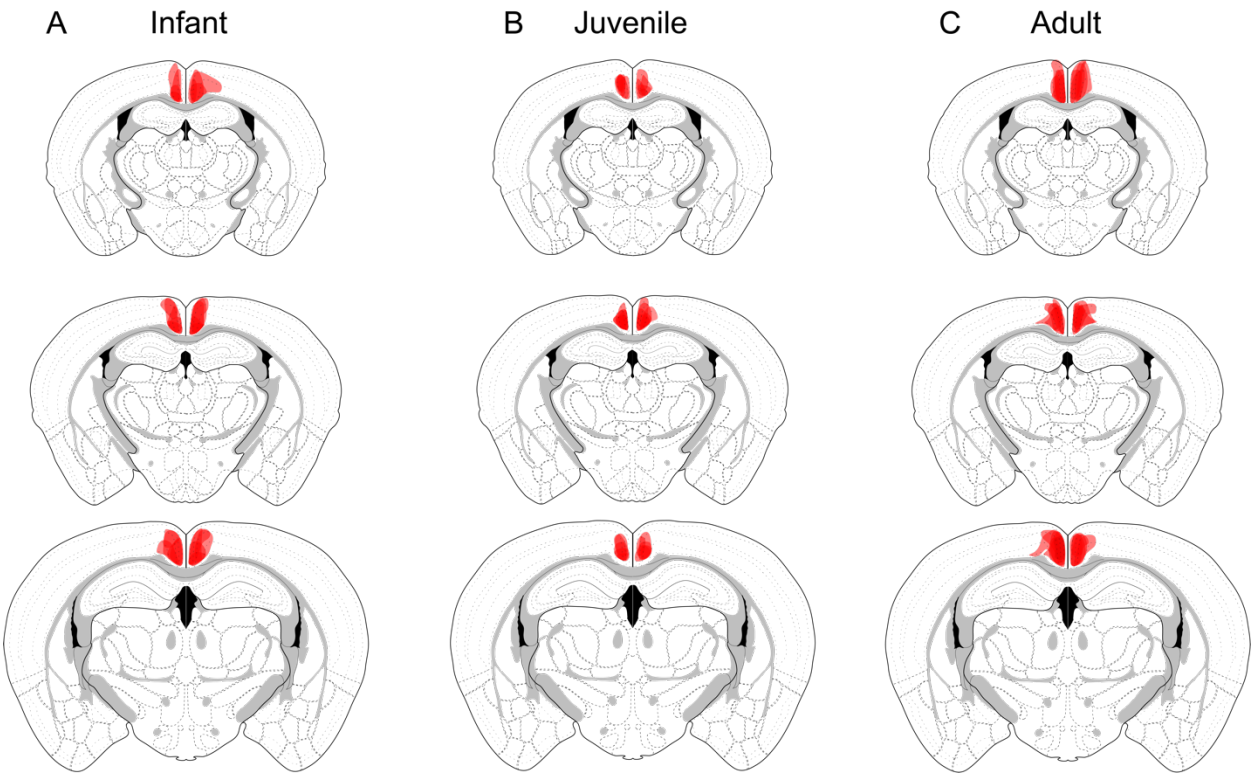

Figure S3. Mapping viral targeting in RSP. Related to Figure 4.
(A) Coronal sections showing location of RSP hM3D-mCherry expression in infant-TRAPed mice
(B) Coronal sections showing location of RSP hM3D-mCherry expression in juvenile-TRAPed mice
(C) Coronal sections showing location of RSP hM3D-mCherry expression in adult-TRAPed mice

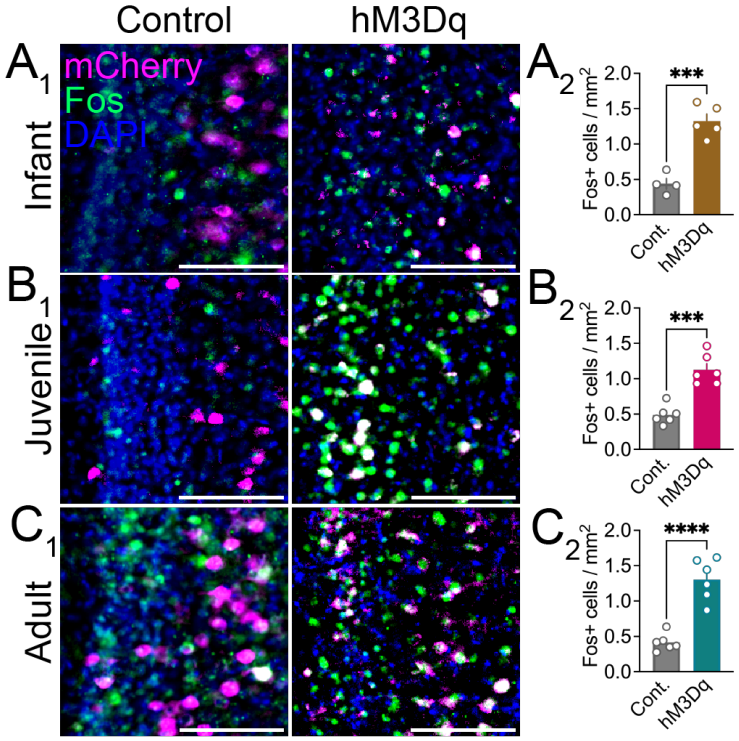

Figure S4. RSP Fos levels in hM3D-expressing vs. control mice. Related to Figure 4.
(A_1) Example images RSP showing AAV-mCherry and Fos+ RSP cells infant-TRAPed mice.
(A_2). Quantification of Fos+ cell density in RSP for infant-TRAPed mice (Cont: N=4, hM3Dq: N=5, P=0.003, two-tailed t-test).
(B_1). Example images RSP showing AAV-mCherry and Fos+ RSP cells infant-TRAPed mice. in juvenile-TRAPed mice (Cont: N=6, hM3Dq: N=6, P=0.0001, two-tailed t-test).
(B_2). Quantification of Fos+ cell density in RSP for juvenile-TRAPed mice.
(C_1). Example images RSP showing AAV-mCherry and Fos+ RSP cells adult-TRAPed mice.
(C_2). Quantification of Fos+ cell density in RSP for adult -TRAPed mice (Cont: N=6, hM3Dq: N=6, P<0.0001, two-tailed t-test).
Scale bars, 125 μm. Graphs show mean ± SEM.

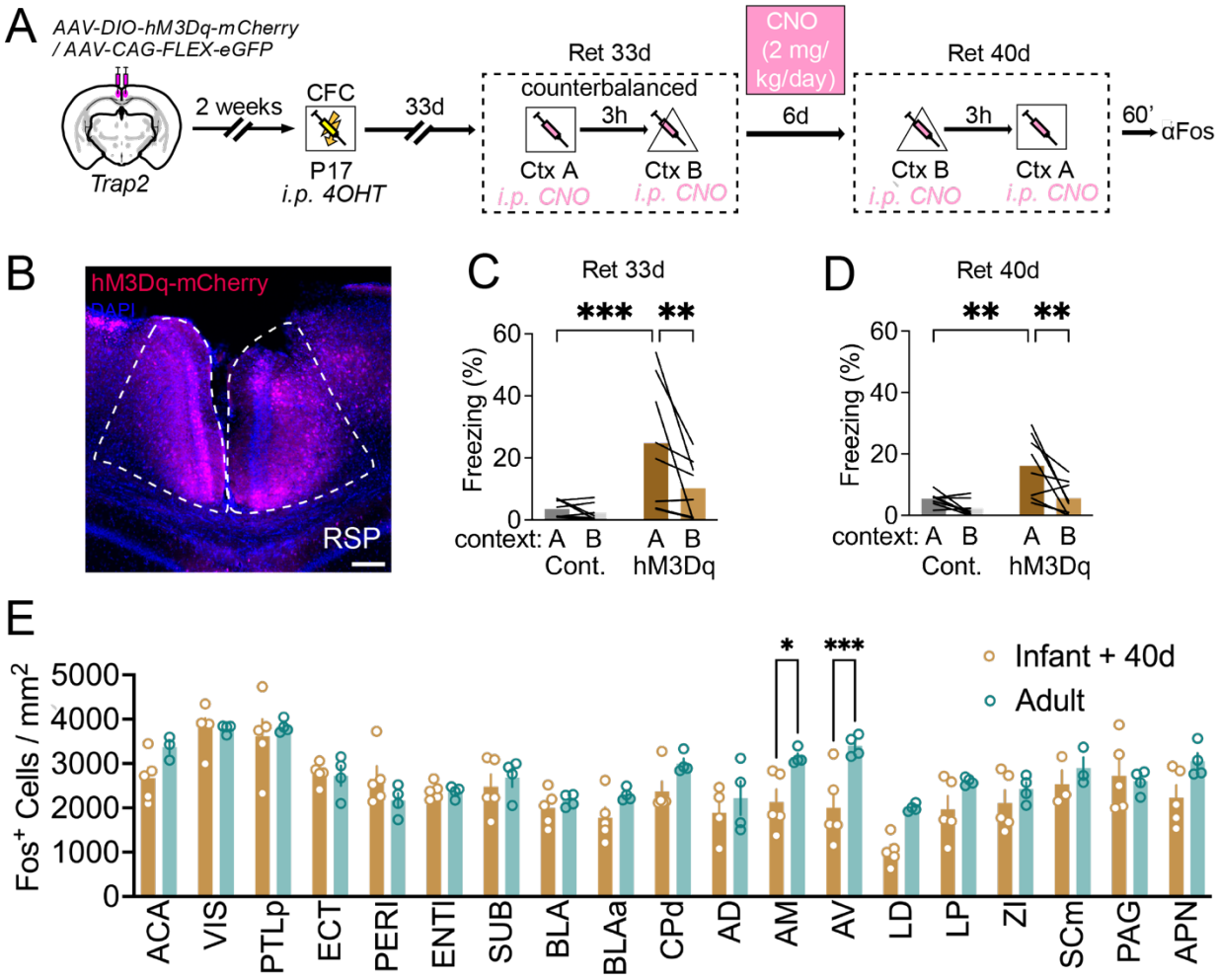

Figure 5. Chemogenetic reactivation of learning encoding ensembles in RSC 33d after training recovers infant memories

(A) Experimental design.

(B) Representative coronal section showing AAV injection site in RSP. Scale bar, 125 µm.

(C) Percent freezing levels in contexts A and B during the 33-day retrieval test in control (gray) and hM3Dq (brown) mice ($F_{virus}(1,14)=9.06$, P=0.009; $F_{context}(1,14)=7.41$, P=0.01; $F_{int}(1,14)=5.23$, P=0.03, Cont: N=8, hM3Dq: N=8, two-way ANOVA with Holm-Sidak posthoc test).

(D) Percent freezing levels in contexts A and B during the 40-day retrieval test in control (gray) and hM3Dq (brown) mice ($F_{virus}(1,14)=9.81$, P=0.007; $F_{context}(1,14)=12.3$, P=0.003; $F_{int}(1,14)=4.65$, P=0.07, Cont: N=8, hM3Dq: N=8, two-way ANOVA with Holm-Sidak posthoc test).

(E) Comparison of regional Fos levels in P17-TRAP+40d vs. Adult TRAP from Figure 4 ($F_{region}(18,121)=18.97$, P<0.0001; $F_{age}(1,7)=3.05$, P=0.12; $F_{int}(18,121)=3.5$, P<0.0001, Inf: N=5, Adult: N=4, two-way mixed effects repeated measures analysis with Sidak posthoc test). Graphs show mean ± SEM. *P<0.05. See also Figures S5 and S6.

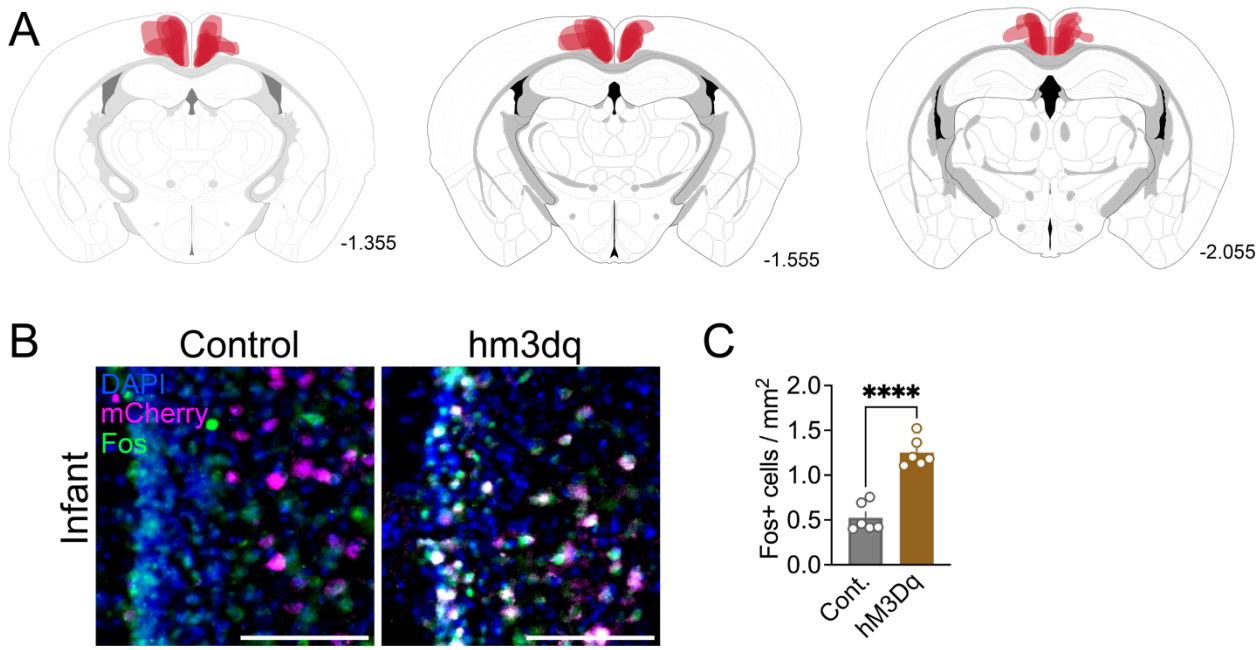

Figure S5. Mapping viral targeting in RSP. Related to Figure 5.
(A) Coronal sections showing location of RSP hM3D-mCherry expression in infant-TRAPed mice.
(B) Example images RSP showing AAV-mCherry and Fos+ RSP cells infant-TRAPed mice. Scale bars, 125μm.
(C) Quantification of Fos+ cell density in RSP for infant-TRAPed mice (Cont: N=6, hM3Dq: N=6, P<0.0001, two-tailed t-test). Graphs show mean ± SEM.

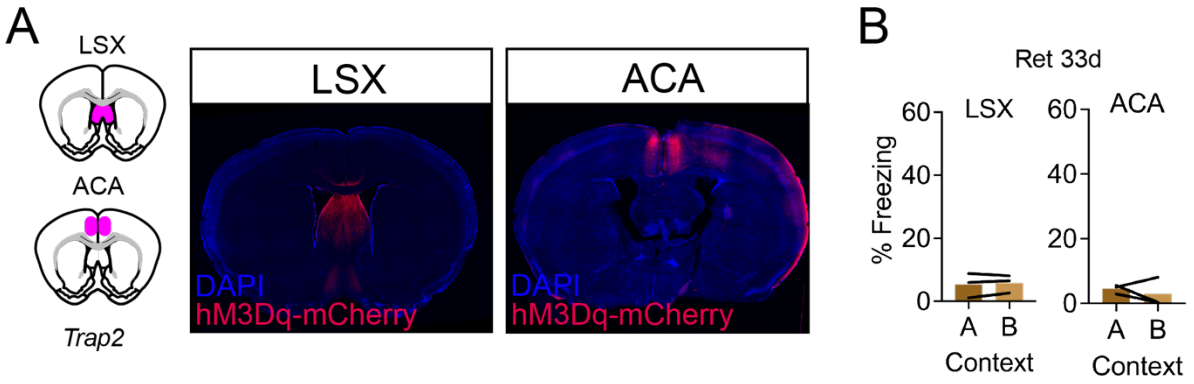

Figure S6. RSP DREADD validation and controls for Figure 5.
(A) Representative coronal section showing AAV-hM3Dq injection sites in LSX and ACA.
(B) Percent freezing levels in contexts A and B during the 33d retrieval test in LSX- and ACA-targeted mice (LSX: P=0.54, N=3, ACA: P=0.56, N=3, paired t-test). Graphs show mean ± SEM.

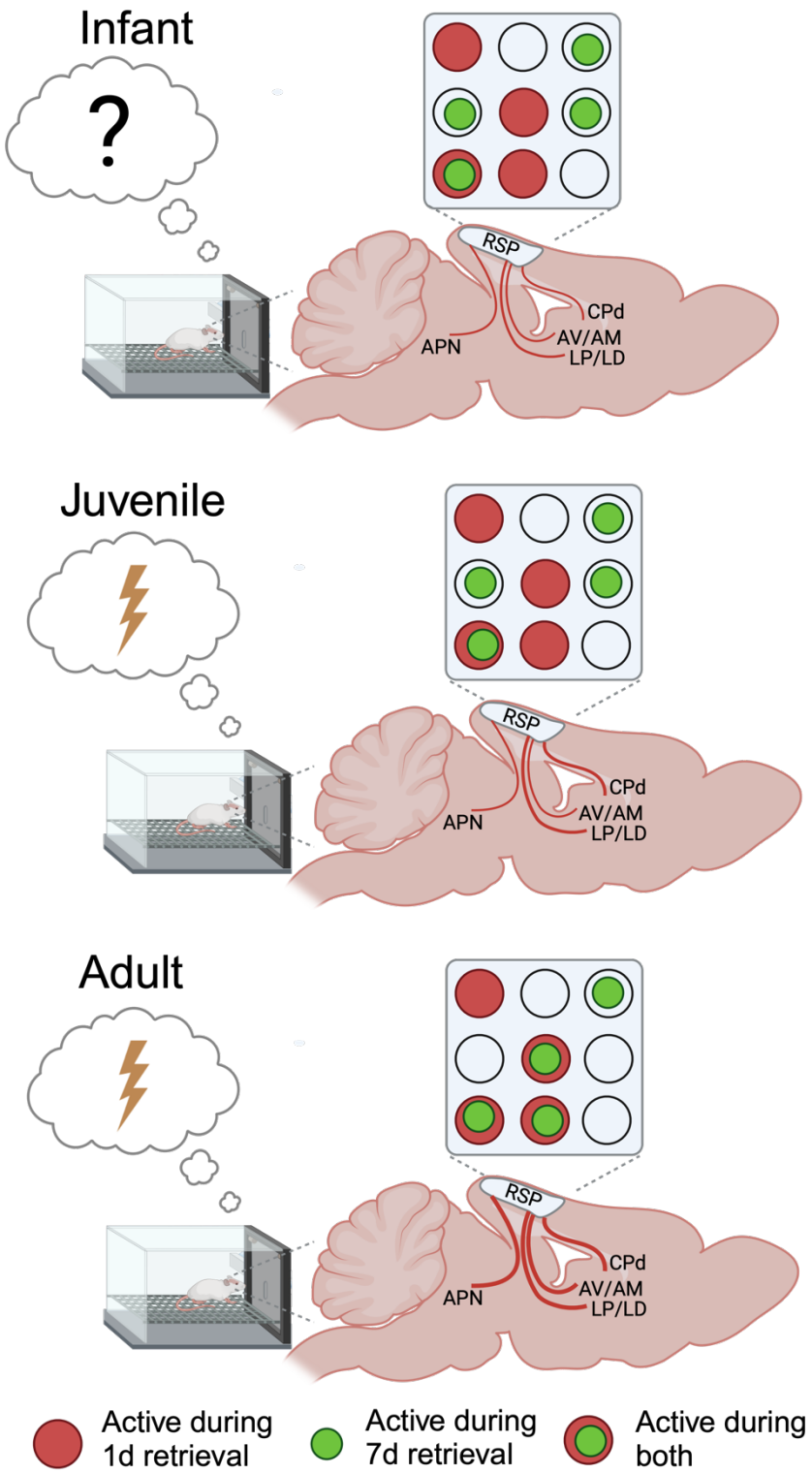

Figure 6. Working model
A progressive maturation of RSP ensemble stability and functional connectivity during memory retrieval underlies the emergence of persistent memories across development.